Study on Performance Enhancement of Lithium-Oxygen Batteries

By

Chengji Zhang

B.Eng., Shenyang Ligong University, 2014

THESIS

Submitted as partial fulfillment of the requirements for the degree of Master of Science in Materials Engineering in the Graduate College of the University of Illinois at Chicago, 2017

Chicago, Illinois

Defense committee:

Dr. J. Ernesto Indacochea, Chair and Advisor

Dr. Hsien-Hau Wang, Co-Advisor

Dr. Michael J. McNallan

Contribution of Authors

Parts of the results represented in Chapter 4, section 4.3 were published as manuscript (Wang, H-H., et al., *Lithium Superoxide Hydrolysis and Relevance to Li-O_2 Batteries.* The Journal of Physical Chemistry C, 2017. **121**(18): p. 9657-9661.) for which I was the fourth author. I helped my research supervisor, Dr. Hsien-Hau, Wang, who is the first author, to correct the calibration curve in Figure 1, and contributed part of the preliminary data in Table 2. I was also contributing to the characterization results regard to pH measuring and analyzing. My work was critical to the conclusions of this manuscript since the results acquired from pH measurement plus the further calculation results strongly justified the validity of the posted conclusion.

Chapter 3 and 4 also represents a series of my own unpublished results directed at developing certain new catalysts for high cyclability Li-O_2 battery. I expect that the research area I was in charge will resume in the laboratory after I leave and therefore this work will be eventually published as part of a co-authored manuscript.

Table of Contents

List of Abbreviation

AC Active Carbon

ANL Argonne National Laboratory

DFT Density Functional Theory

DMC Dimethyl Carbonate

DME Dimethoxyethane

EV Electric Vehicles

GO Graphene Oxide

HEV Hybrid Electric Vehicles

NMP N-methyl-2-pyrrolidone

OCV Open-circuit voltage

OER Oxygen Evolution Reaction

ORR Oxygen Reduction Reaction

PVDF Polyvinylidene Difluoride

RGO Reduced Graphene Oxide

GHG Greenhouse Gas

SEI Solid-Electrolyte Interfaces

SP Super P Carbon

TEGDME Tetraethylene Glycol Dimethyl Ether

Summary

The electrification of transportation is well-recognized as alternative strategies to minimize the dependence on fossil fuels and eventually address the effects on Climate change. Among all strong candidate for the next generation energy storage technology, the lithium-air battery has attracted exclusively attention in terms of its high theoretical energy density, which is even comparable to gasoline combustion. And as a result, makes it promise for powering the fully battery powered Electric Vehicles (EVs). However, the high overpotential while redox reaction happens between charge and discharge is the enormous challenges obstructed the way to success. On the other hand, electrolyte and electrode decomposition was almost inevitable as the battery keeps cycling and eventually leads to cathode clogging which is in responsible for poor energy efficiency as well as limited cyclability after testing.

In this research, in order to achieve highly desirable battery developments, we first introduce Ir_3Li, a lithium intermetallic, as new catalyst material that helps stabilize the formation of LiO_2, a meta-stable intermediate product instead of the commonly reported Li_2O_2 after discharge, and as a result mechanically reducing the energy barrier. In addition, the way to fabricate improved carbon black cathode and other performance perfection technique were also investigated. Different characterization techniques including SEM, Raman, and titration will be employed to investigate the morphology as well as the distribution of redox products. Along with battery cycling test, these investigation helps better understand the two-step mechanism of the Li-Oxygen battery system.

With the help of all these characterization and justification, an improved Li-O_2 cell will be presented with an energy efficiency of 70% for more than 70 cycles with only moderate capacity loss. At the same time, the discharge products are believed to be Lithium superoxide as wanted instead of Lithium peroxide. As a result, the improved Li-O_2 battery has been successfully explored that could keep running continuously for more than eight weeks.

1. Introduction

1.1 The global energy demand and its effect

It is well known that the energy consumption and climate change are strongly dependent on each other since the total energy consumption by human beings is 20 TW nowadays (showed in Figure 1.1). By 2040, renewables still provide less than 5% of the world's energy demand. Oil, coal, and gas continue to dominate, as expected. The numbers for it is predicted to double in 2050 and eventually triple by the end of this century [1-3]. Nowadays, the fossil fuel is the predominant of 34% of all primary energy source that supplied over 85% of the energy demand all over the world and accounts for 40% of total CO_2 emission [1, 4], which is the acknowledged cause of Global Warming [3].

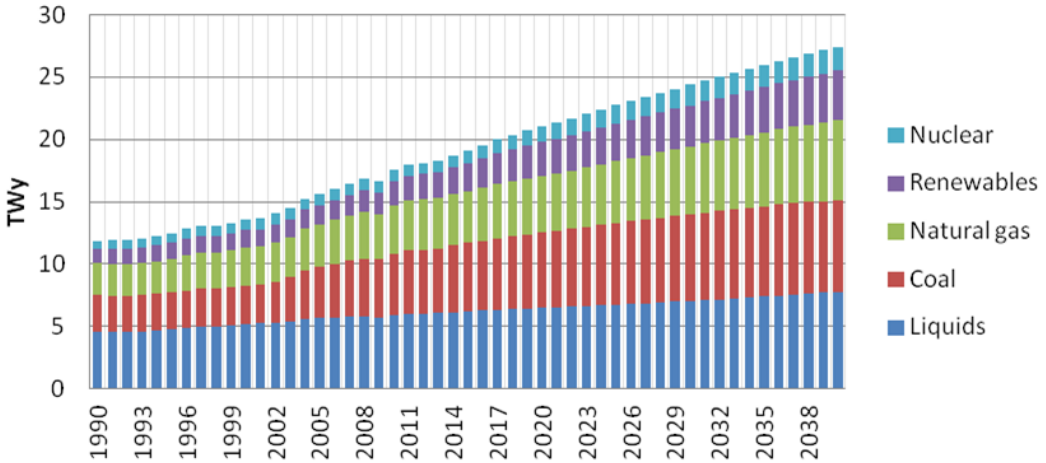

Figure 1.1 Annual projection of global energy consumption forecast (copyright © US Energy Information Agency)

The rising energy demand is putting pressure on non-renewable resources, which in

return bring a negative effect on the global climate with rising quantities of greenhouse gases, mainly CO_2, that are released into the air. While the challenge of climate change is critical, the continuous energy demand is resulting in a shortage of power resource resulting in declining fossil fuel reserves. [1, 2, 5-8].

Under the urgent demanding of fossil fuel crisis, first enacted by Congress in 1975, Corporate Average Fuel Economy (CAFE) Standards [9] was established with the purpose of reduction of energy consumption by increasing the fuel economy of cars and light trucks. The CAFE standards are fleet-wide averages that must be achieved by each automaker for its car and truck fleet each year, since 1978. After it was proposed, automakers were regulated to design their product process higher fuel-efficient, which in return improves U.S. energy security and saves money for each consumer as well as reduces greenhouse gas (GHG) emissions.

On the other hand, Richard P et al. [1] stated that along with the rising climate concerns, exploring and developing renewable energy sources becomes crucial. However, the total powers generated through these techniques are unable to manage or predict. In consequence, the merit of energy storage technologies becomes necessary for satisfying the future power delivery demand of renewable energy.

1.2 The Energy Storage System

Energy storage means the reservation of energy source that generated one time yet to apply at a later time as needed. It plays a predominant role in our daily life to satisfy the enormous demanding for energy consumption by multiple purposes, electrical mostly. After the electricity was found, people have been seeking over decades to find reliable ways to store it as demand. Over the last century, there have

been multiple industrial investigations to explore the processing energy storage requirements as well as merits by technological research (as presented in Fig 1.2 below). Because the Energy storage systems giving us wider option while managing our power supply as for creating a more resilient energy infrastructure and bring cost savings to utilities and consumer.

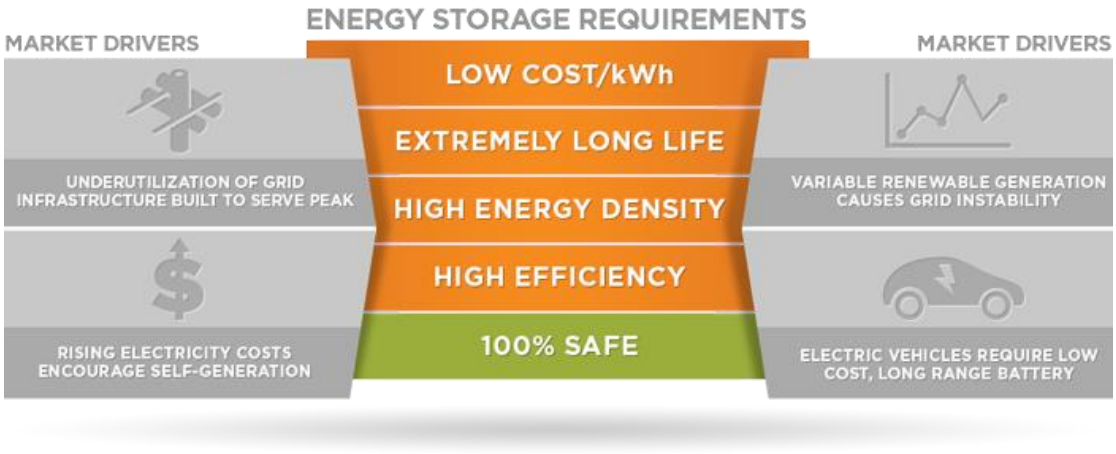

Figure 1.2 Demand and requirement of energy storage application (Source: Eos Energy Storage © 2014).

1.3 History of battery

If we name the list of contributions of innovators and researchers who created our understanding of electricity, Alessandro Volta[1] is always considered the paramount one since it is him who invented the original battery along with the entire field of electrochemistry in 1800. Along with his research, a battery is defined by researchers [10] as the device which consists one or more electrochemical cells that convert stored chemical energy into electrical energy. Each cell contains a positive terminal

[1] Alessandro Giuseppe Antonio Anastasio Volta, February 18 1745 – March 05 1827. Italian physicist and chemist, inventor of the electrical battery.

(cathode), and a negative terminal (anode). Electrolytes allow ions to move between the electrodes, which allows current to flow out of the battery to perform work.

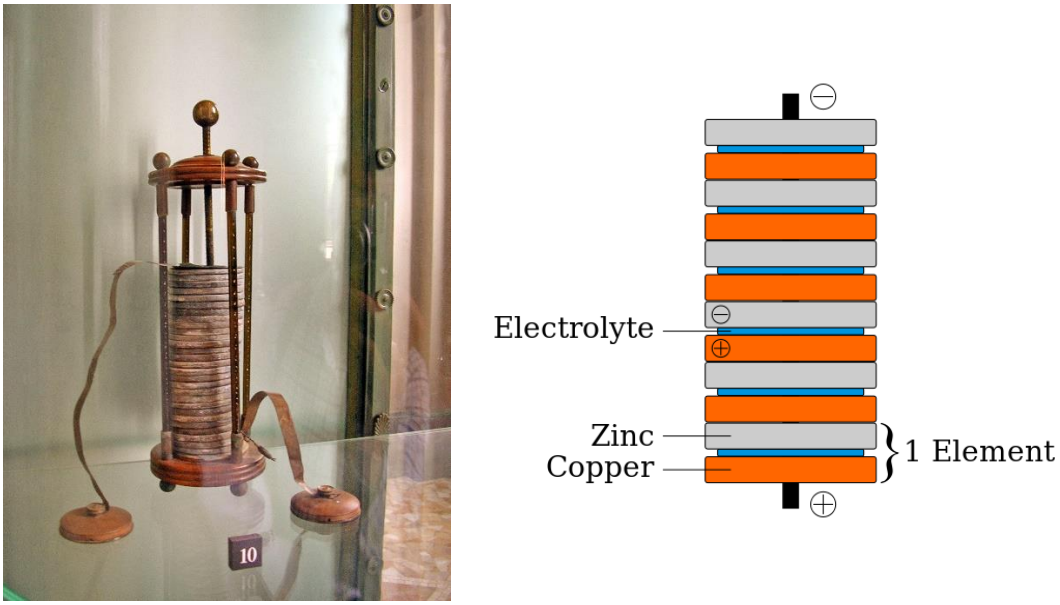

(a) (b)

Figure 1.3 (a) Picture of an Alessandro Volta's electric battery (Tempio Voltiano in Como, Italy). (b) Schematic diagram of a copper–zinc voltaic pile (Source: Wikimedia 2015).

As shown in Figure 1.3, for the very first battery set called voltaic pile, the battery designed by Volta[1] only consist of stacked discs of Zn and Cu separated by cardboard or felt spacers soaked in salt water (the electrolyte). It meant to act an inevitable rule in the future in terms of the dependency of electrical power after the Second Industrial Revolution. Unsurprisingly, they are now so ubiquitous today that almost invisible to us as the demand for consumption arises rapidly every year and eventually bring a cleaner and safer life.

1.4 Rechargeable battery and its application

1.4.1 Introduction of rechargeable batteries

A rechargeable battery, also known as a *secondary cell*, is widely used in the 21st century as one of the major energy storage technique that powering those portable devices, like handsets, laptops and even automobiles. After Gaston Planté[2] first invented the applicable lead-acid batteries in 1859, the eyesight of researchers started to shift and various types of battery systems have been developed then. Other than fully charged before supplied and one-time discharging after consumed for dispensable battery (also known as a primary cell), a rechargeable battery can always run multiple cycles from charging and discharging in terms of irreversible electrochemical reaction.

There are various combinations of electrode materials and electrolytes being studied [11], like nickel cadmium, lithium ion, nickel metal hydride, lead–acid and lithium ion polymer. Secondary batteries also available in various sizes and shapes, distributing from coin cells to megawatt grids. In addition, there is some rechargeable battery that is designed by same sizes to replace the disposable one in terms of its interchangeability.

1.4.2 Transportation application with rechargeable techniques

Compared to the prototype rechargeable batteries, the cell performance has been perfected tremendously these days; however, the cell capacity is still considered

[2] Gaston Planté, April 22 1834 – May 21 1889, famous as the inventor of lead-acid battery in 1859, which eventually became the first rechargeable battery for commercial use.

insufficient for EVs and portable devices, which is the most urgent demanding for current electrochemical research and development. Yamamoto, O et al. [8] pointed out that the energy capacity of the first invented lead-acid battery calculated from the active material mass and the open-circuit voltage (2.05V) is 171 Wh kg^{-1}, which leads to an operation capacity of not more than 100 km of a lead-acid powered EV per charge. As a result, the focusing of rechargeable batteries shifted to the Li-ion battery system.

Literally, rechargeable batteries always possess lower environmental impact of use and higher economic efficiency than non-rechargeable (disposable) batteries. That means other than higher initial cost, rechargeable batteries can recharge cheaply and used many times. Some rechargeable battery types are available in the same form factors as disposables. To make a summary, the utilization of electric transportation would not only help reduce CO_2 emissions and thereby containing the climate change but also raise the fuel efficiency and thus become more popular in the US.

1.5 Lithium-Oxygen batteries

1.5.1 Introduction

Nowadays, in order to satisfy the nourishing demand of portable electronic applications such as portable electronic, electrical vehicles (EVs) and hybrid electric vehicles (HEVs), there has been intensive investigations done by researchers for building an environmentally friendly, high-efficiency and long cycle life energy-storage system. Supercapacitors (SCs) are considered to be one of the valuable competitors in terms of its vast power capability, long cyclability (>100,000 cycles), as well as low, keep up cost and fleet dynamics of charge propagation.

However, compared to lithium-ion batteries, SCs are still not the top choice when delivering high energy density capacity is acquired [12]. However, as shown in Fig 1.4, current Electrical Vehicles (EVs) like Tesla or Nissan Leaf that powered by lithium-ion can only operate for 200 Miles per charge at most, which could barely meet the needs of ideal demand that could replace the gasoline-powered IC engine. Therefore, lifting-up the capacity performance of new energy storage technique become to be developed to catch up or even beyond that of batteries.

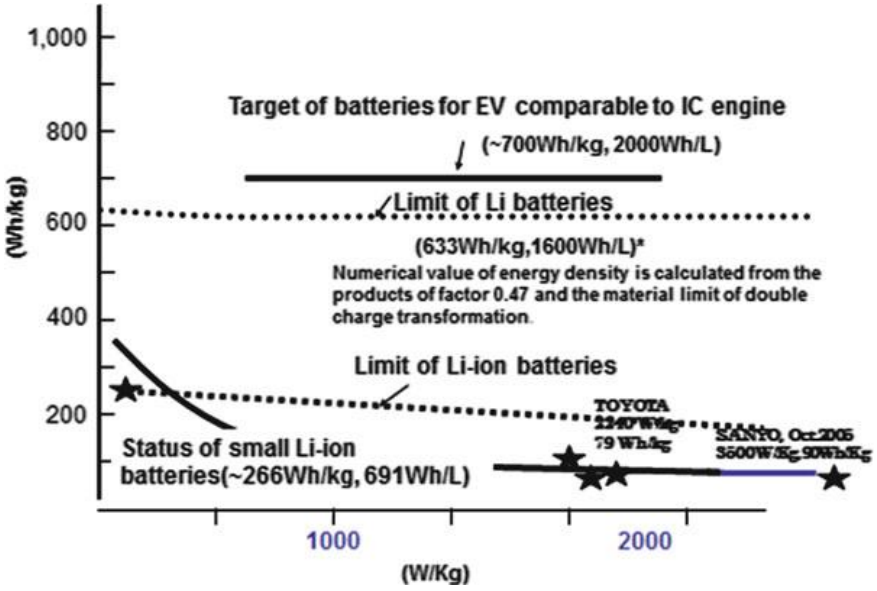

Figure 1.4 Status and targets of advanced batteries. Reprint from ref [13].

The Li-O_2 batteries possess far higher theoretical energy densities which are three to five times larger than the commercial Li-ion batteries [2, 5, 6, 11, 14, 15]. The Li-O_2 battery was invented first-time by Littauer and Tsai in 1976 [16]. However, this research was suspended during the late 80s with the reason of critical side reaction of lithium with water in electrolytes; one decade later, the prototype of the first rechargeable Li-O_2 battery was eventually reported by Abraham et al. [17] in 1996, which incorporated an organic electrolyte instead of aqueous one.

The high theoretical energy capacity of the Li-O_2 battery is explained by cathode oxidant, O_2, is obtained from the external circumstance instead of the electrode itself [11]. Ideally, a higher battery density is attributed to the large chemical potential gap between two electrodes as well as minimize the electron involved per exchange while cycling [18]. When it comes to Li-O_2 battery, since both the atomic mass and the electronegativity of Li-foil anode is low, the electrons involved during redox are transforming more easier than other metals while exchanging the positive-ions [2]. In addition, if we just consider the atomic mass of Li metal itself, the gravimetric power density of Li-O_2 battery regards to the anode becomes higher than 13,000Whkg^{-1} (excluding oxygen is as high as 11,430 Whkg^{-1}) which is comparable to the energy density of gasoline (13,200Whkg^{-1}) [6, 8].

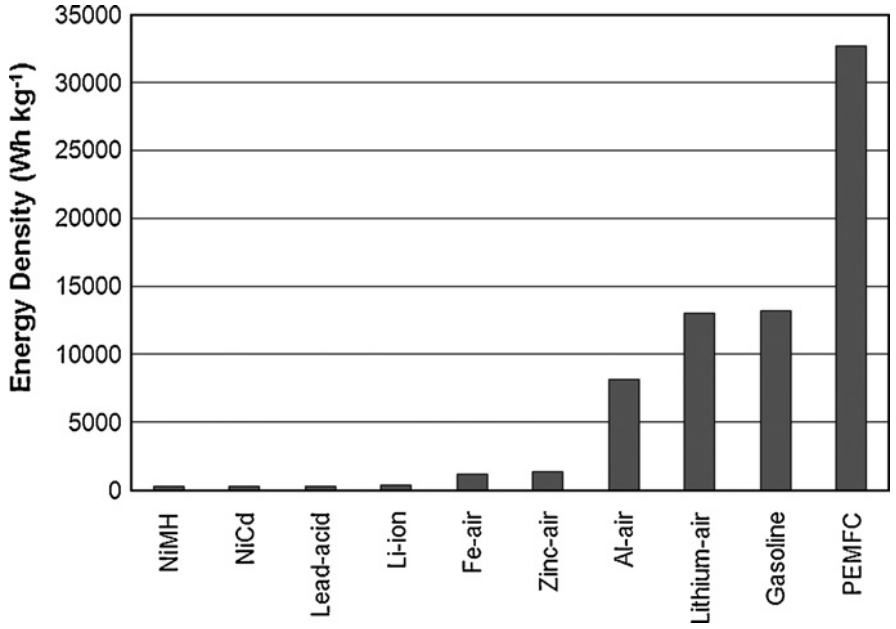

Figure 1.5 Current and developing energy storage technologies and the comparisons of their respective theoretical energy densities. Reprint from ref [1].

So far, there have been four types of chemical architectures investigated for Li-O_2 batteries which include three different versions of liquid electrolytes: aprotic organic electrolyte, aqueous electrolyte and a mixed system with separate electrolyte that immersing each electrode. The fourth type of Li-O_2 batteries includes a solid electrolyte [2, 5, 6, 19]. In addition, Figure 1.6 presents the all four different architectures of Li-Oxygen batteries, where each of them uses lithium foil as the anode.

For all types of Li-O_2 batteries using liquid electrolytes, a stable solid electrolyte interface (SEI), either artificial or spontaneously formed, will exist between lithium surface and electrolyte to protect the Li anode. In typical aprotic Li-O_2 batteries, the lithium metal anode will contact with the electrolyte and eventually developed a steady SEI layer that passivated the anodes from overreaction. This circumstance is similar to the properties and mechanism of how SEI layers formed in conventional Li-ion batteries with lithium-carbon electrode [4].

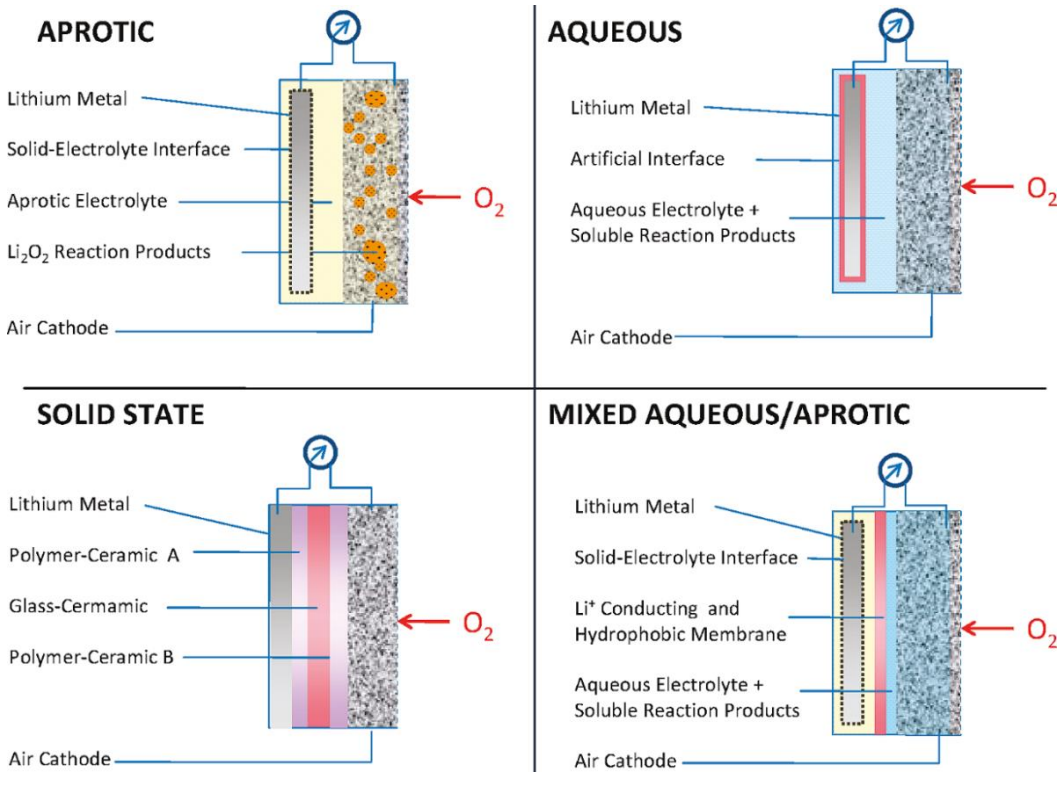

Figure 1.6 Principal components of all 4 types of Li-O_2 batteries. Spontaneously formed SEIs that are shown as dashed lines, whereas artificial SEIs are marked as solid lines. Reprint from ref [2].

Although all four prototypes of the Li-O_2 battery have been released and investigated for several years by researchers and each type of them has its own advantages, only the one with aprotic electrolyte has attracted researchers the most worldwide due to its promised electrical rechargeability. As for secondary battery designed for the specific purpose of alternate sources for automobile, the capacity of multiple-time utilization is a must. Thus, only the aprotic Li-O_2 battery will be tested and discussed in this thesis.

1.5.2 Mechanics of Li-O_2 Battery

Since only aprotic electrolyte has been utilized in this research, we will focus on the electrochemical mechanics of aprotic cell only. The Aprotic Li-O_2 battery usually consists of a porous Carbon fiber substrate cathode in order to promote gas permeability of Oxygen while ORR and OER and pure Lithium metal anode, as shown in Fig 1.7. The electrodes are normally separated by glass fiber separator that is immersed in Li^+ conducting electrolyte.

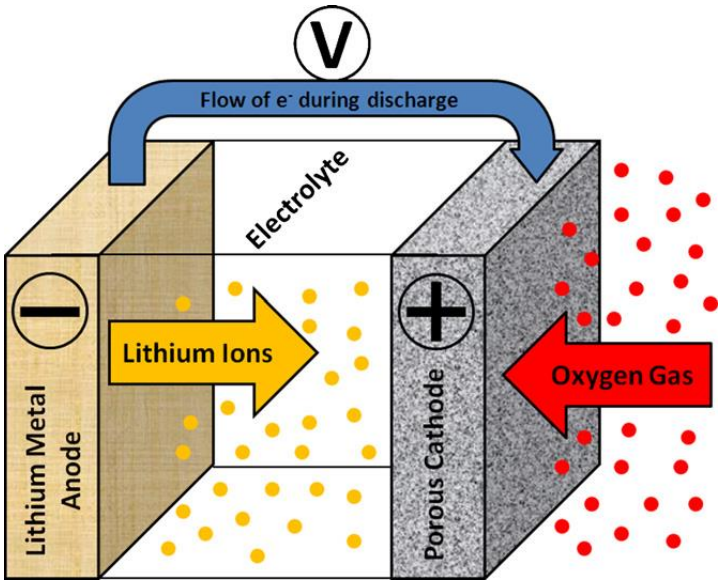

Figure 1.7 Schematic diagram presents how the redox reaction happens for both Lithium Anode and Porous Carbon cathode. Reprint from ref [1].

In the anode side, there is simple electron transportation by Lithium on Anode side that showed in reaction (1). For the cathodic side, the electrochemical reactions are not following a one-step process while discharging [1, 2, 4, 20]. In addition, the battery mechanics are not well developed via the previous investigation. However, most of the people believe that the Li-O_2 battery follows a two-step reaction with the discharge products of LiO_2 and Li_2O_2 that has been first stated by Hummelshoj et al. [20]. In Hummelshoj's work, they were using density functional theory (DFT) to describe the electrochemical reaction while discharging. As been shown in reactions (2) and (3), the discharge products for those two reactions are LiO_2 and Li_2O_2, respectively. The intermedia product, LiO_2, has been cited as a surface site on Li_2O_2 where the reaction proceeds.

$$Li_s \rightarrow Li^+ + e^- \quad \text{(Anode)} \tag{1}$$

$$Li^+ + e^- + O_2 \rightarrow LiO_2 \quad \text{(Cathode)} \tag{2}$$

$$Li^+ + e^- + LiO_2 \rightarrow Li_2O_2 \quad \text{(Cathode)} \qquad (3)$$

Literally, the most desirable reaction in aprotic Li-O_2 should be reaction (4) with lithium oxide (Li_2O) as full reduction product in terms of higher specific energy and energy density [4]. However, the multiple reactions involved from Li to Li_2O would only exist under low cutoff Voltage at 2.0V (vs Li/Li^+) or below that responsible for the electrolyte decomposition. Besides, as intrinsic nature of insulated Li_2O_2 involved, the subsequent formation of Li_2O are less likely to be reached. Thus, Li_2O_2 was observed as discharge products for most of the research. Reaction (5) provides another method as for achieving the Li_2O_2 as reported.

$$2Li^+ + 2e^- + Li_2O_2 \rightarrow 2Li_2O \quad \text{(Cathode)} \qquad (4)$$

$$LiO_2 + LiO_2 \rightarrow Li_2O_2 + O_2 \quad \text{(Cathode)} \qquad (5)$$

Although the stability of LiO_2 is weak and no one has ever announced the successful way to synthesize high purity crystalline end product, Lu et al. [21] asserted that the LiO_2 could be stabilized by using certain graphene-based cathode while discharging in Li-O_2 battery system, at the same time, Xie, J et al. [22] also states that they can run the Li-O_2 battery through a one-electron process showed in reaction (2) with certain ionic liquid electrolyte. Those related research results strongly supported Hummelshoj's two-step process hypothesis.

On the other hand, another well-acknowledged method along with aqueous electrolyte was investigated by Tao L. et al. [23] whose announced that the battery can be charged and recharged through forming and removing crystallized LiOH and eventually resulting in an energy efficiency of 93.2% and yielding an overpotential of only 0.2 Volt. The battery is believed to process high tolerance of water, which

provides dominant source of OH anion together with lithium iodide while cycling. LiI presents itself as a redox mediator for this kind of Li-O_2 cell along with LiOH. The chemical mechanism is listed as two-step reactions for both OER and ORR occurs as he proposed in reaction (6) to (9).

$$4Li^+ + 4e^- + 4O_2 \rightarrow 4LiO_2 \quad \text{(Cathode)} \tag{6}$$

$$4LiO_2 + 2H_2O \rightarrow 4LiOH + 3O_2 \quad \text{(Cathode)} \tag{7}$$

$$6I^- \rightarrow 2I_3^- + 4e^- \quad \text{(Anode)} \tag{8}$$

$$4LiOH + 2I_3^- \rightarrow 4Li^+ + O_2 + 6I^- + 2H_2O \quad \text{(Anode)} \tag{9}$$

The electron/LiOH molar ratios during discharge and charge are both equal to one. Besides, reaction (6) and (8) are chemical reactions whereas reaction (7) and (9) are electrochemical reactions. By using an rGO electrode and the redox mediator LiI, in a DME-based electrolyte, Liu demonstrated a highly efficient, rechargeable Li-O_2 battery with extremely large capacities [23, 24].

1.5.3 Limit and Challenges

While successful operations of Li−O_2 batteries are considered as the next generation energy storage technique. However, it has always been challenged by certain limitations that impede its application regards to intrinsic issues.

First, the weight of oxygen must be included for the Li-O_2 battery system, because part of the discharge product is stored in the battery. Ideally, the batteries rather work with oxygen that exists in the atmosphere, since the Li-O_2 battery is specifically designed for Electrical vehicles (EV's). However, the air components except oxygen

are mostly considered impurities which will cause cell damage while cycling. For instance, lithium can react with N_2 (78% in concentration in the air) causing the electrode decomposition. In another word, all four configurations will encounter the difficulties of developing a high-throughput air-breathing system that passes no contaminations except O_2. In this research, for eliminating uncertain variables, we choose to study the battery mechanisms with pure oxygen.

As we mentioned above that the Li-O_2 system possesses high energy density of about 11,430 $Whkg^{-1}$, which is comparable to that of the fossil fuels. The practical energy density is far less (Only about 40 to 50%) than the theoretical in terms of technical and intrinsic limitations, however. Besides that, the power density (measured in W kg^{-1}) and the current density in regards to the recent investigation [8, 20] remains very low. Furthermore, the Li-O_2 battery is reported to have the capacity as high as 3000 $mAhg^{-1}$ with minor energy lost with no more than a critical current density of 1 $mAcm^{-2}$ [17, 21, 22, 25-27]. However, an increase of one order magnitude or more in current density would provide enough power needed for the operation of Electrical Vehicles. This had barely achieved in any recent investigation [2, 15, 19, 28].

An overpotential indicates the potential difference, ΔE, between a theoretical or thermodynamically determined voltage (ΔE^0) and the actual voltage under operating conditions. The theoretical potential could be determined by Nernst equation stated in equation (10).

$$\Delta E = \Delta E^0 - \frac{RT}{nF} \ln Q \tag{10}$$

Where R is the gas constant (R= 8.314472 $JK^{-1}mol^{-1}$), T is the temperature in kelvins. n is the total number of involved electrons transferred during the reaction. F refers to

Faraday constant (96,500 C/mol); the last one, Q, means the reaction quotient of the cell reaction. Since the redox reactions happened on the electrode are confined by intrinsic factors that affect the reaction kinetics, we would expect both charge and discharge potentials derived from the standard potential (ΔE^0) and this would be explained because of overpotential. The overpotential is the extra energy required based on specific kinetics to drive the reaction forward, a fast reaction with high current density normally encounters lower overpotential whereas a slow reaction with low current density always faced with higher overpotential.

Current Li-O_2 cells are limited by high overpotentials and low cyclabilities. For example, Fig 1.8 shows how the charge potential is considerably higher than the discharge potential, which gives overpotentials of more than 1.5V combined for the cell system. Consequently, the cyclability, as well as capacity, is limited in terms of low electrical energy efficiency, which is only 60-70%, while an efficiency of more than 90% is the selection criteria for practical propulsion batteries or commercialized batteries, like Li-ion battery.

Furthermore, as shown in the same Fig below, the non-catalyzed aprotic Li-Oxygen battery only runs for 4 cycles from the earlier attempt. Previous Li-oxygen cells have been operated by up to about 50 cycles with moderate loss in capacity [29], and lately it has been improved to 100 cycles [14, 30, 31], but it is far short for commercial capacity utilization in Electrical Vehicles, that require over 500 cycles with a moderate capacity loss. Li-ion batteries with $LiCoO_2$ and $LiFeO_4$ as the cathode are the commercial battery type used. Therefore, future research efforts need to focus on improving the capacity retention during cycling.

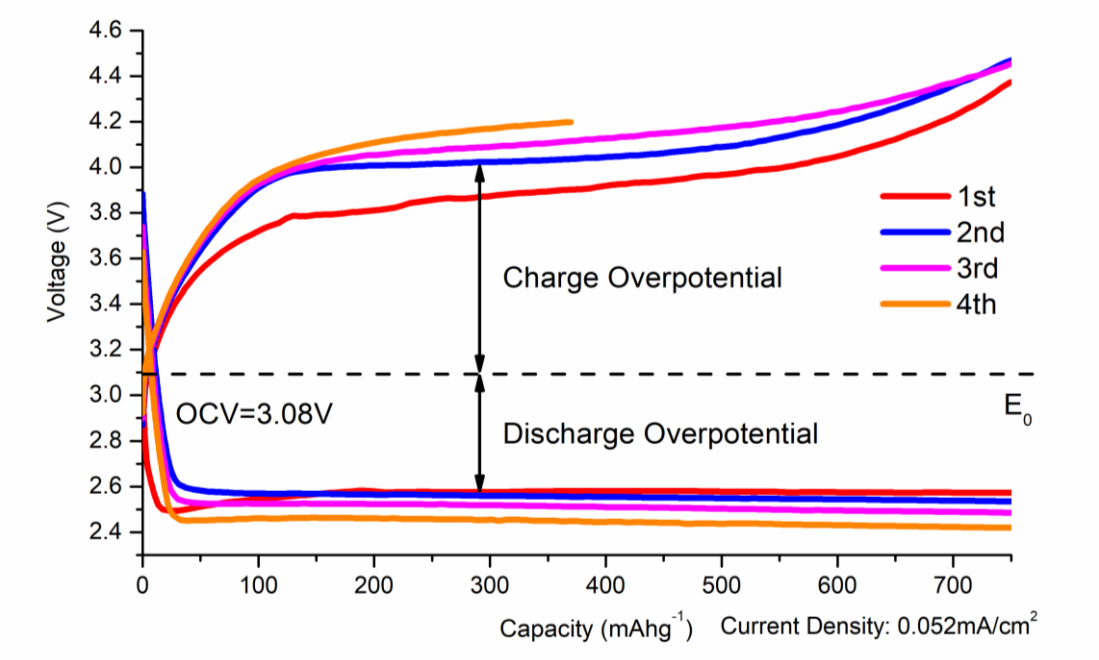

Figure 1.8 Cycling performance test of a Li-O_2 battery with aprotic electrolyte and non-catalyzed rGO cathode. The cell runs for only 4 cycles which reveals the necessity of catalyzing employment.

Factors that affect the overpotentials, as well as the low cycle life of Li-Oxygen cells, have been briefly described by P. Richard et al. [1] and G. Girishkumar et al. [2]. In aprotic Li-Oxygen systems, the existence of positive overpotential on charging is explained by additional energy required to reverse the occurred reaction while discharging, since the reduction products (normally reported as Li_2O_2) are considered indissoluble. While reduction reaction proceeds, the accumulation of discharge product, Li_2O_2, decrease the internal conductivity of the electrode as well as negatively affect the reaction kinetics. These are reflected out by the existence of negative overpotential. After the porous cathode surface got clogged by discharge products, the rate that the cathode get insulated or passivated will determine the certain actual capacity of the cell. Under these circumstances, a variety of catalysts was utilized as it can help decrease the overpotentials to standard potential value and hence the asymmetry decrease observed in the charge/discharge curve.

1.5.4 Current approach

It has been reported by several groups [15, 19, 32] that the overpotential could be substantially reduced by the choice of variety of catalyst for both electrode and electrolyte. S-H Yang et al. [32] demonstrated this decrease in asymmetry of Li-O_2 battery by applying platinum–gold/carbon (PtAu/C) as a bifunctional catalyst for carbon cathode. The result reveals that by using certain catalyst, the voltage required to reverse the discharge products back to Li metal and O_2 has been efficiently reduced.

Similar results were demonstrated in Fig 1.9 as given by Lu et al. [21] where they compare typical charge/discharge curves of lithium-oxygen batteries with and without nano-size Iridium metal catalysts. In particular, the introduction of the catalyst improves the cyclability from 9 to 40 cycles by effectively enhancing the electrical energy efficiency from 65% to 80% at a capacity of 1000mAhg^{-1}. These investigations support an idea that the extra energy barrier is in responsible for the conclusion that overpotential can be substantially reduced by utilizing different catalyzed cathodes for Li-O_2 batteries.

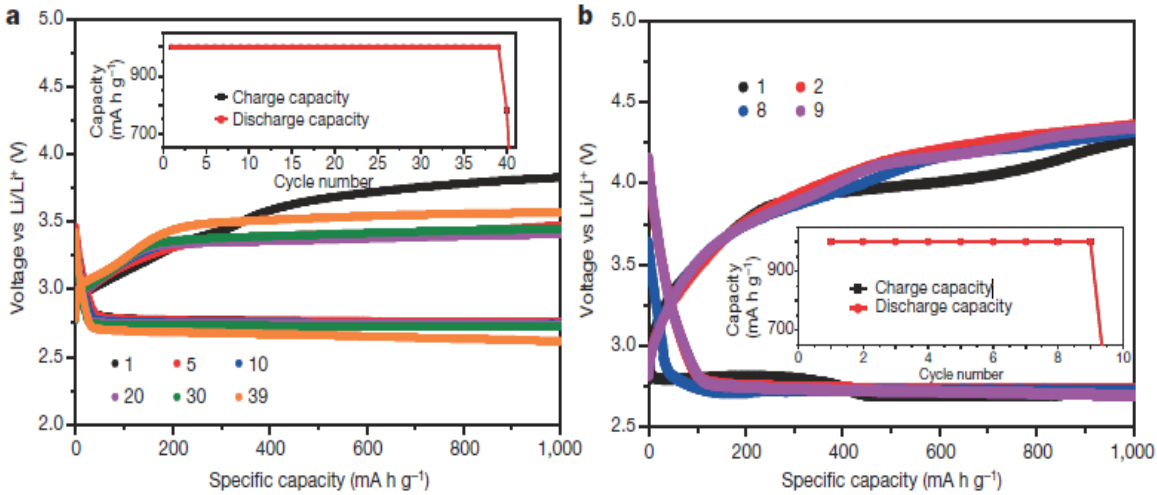

Figure 1.9 Electrochemical tests for Voltage profiles of the Ir–rGO cathode. Cycle number of voltage plot is given by the color of the plotting symbol. Inset shows capacity as a function of cycle number. b, Voltage profiles of the rGO cathode. Cycle number of voltage plot is given by the color of the plotting symbol. Inset shows capacity as a function of cycle number. Reprint from ref [21].

Bruce, P. G.et al. [33] incorporated a redox mediator called tetrathiafulvalene (TTF), which enables the battery to recharge at rates that are unable to reach normally. During charge, TTF is oxidized to TTF^+ at the cathode surface; the TTF^+, as a result, oxidizes the solid Li_2O_2, which results in the regeneration of TTF; The mediator acts as an electron-hole transfer agent that permits efficient oxidation of solid Li_2O_2. The cell with the mediator reported 100 charge/discharge cycles with low current density. This gives an idea of the cell performance could be also improved by modified electrolytes.

In my area of interest, the noble metal/intermetallic was introduced as the catalyst for enhancing the efficiency as well as cyclic performance. The cell with selected electrode and catalyst runs for more than 70 cycles with minor capacity loss. On the other hand, the total cyclic testing time was calculated to be more than 8 weeks, this combined with the careful selection of electrolyte makes this Li-O_2 study promising to contribute knowledge for battery commercialization in the near future.

2. Experimental preparation

2.1 Cathode materials preparation

The cathode materials can be chosen from a variety of materials [2, 8, 28]. In this research, the self-fabricated reduce Graphene Oxide (rGO) were used as active carbon cathode materials because of its high conductivity, high surface area and relatively low cost. Originally, the reduce Graphene Oxide has been synthesized from Graphite Oxide, which is the oxidation product of commercial graphite flakes. The mechanism was explained in Fig 2.1. The pristine and catalytic cathode was fabricated by coating the conductive carbon slurry on top of the surface of conductive carbon paper (Sigracet® GDL 35BC).

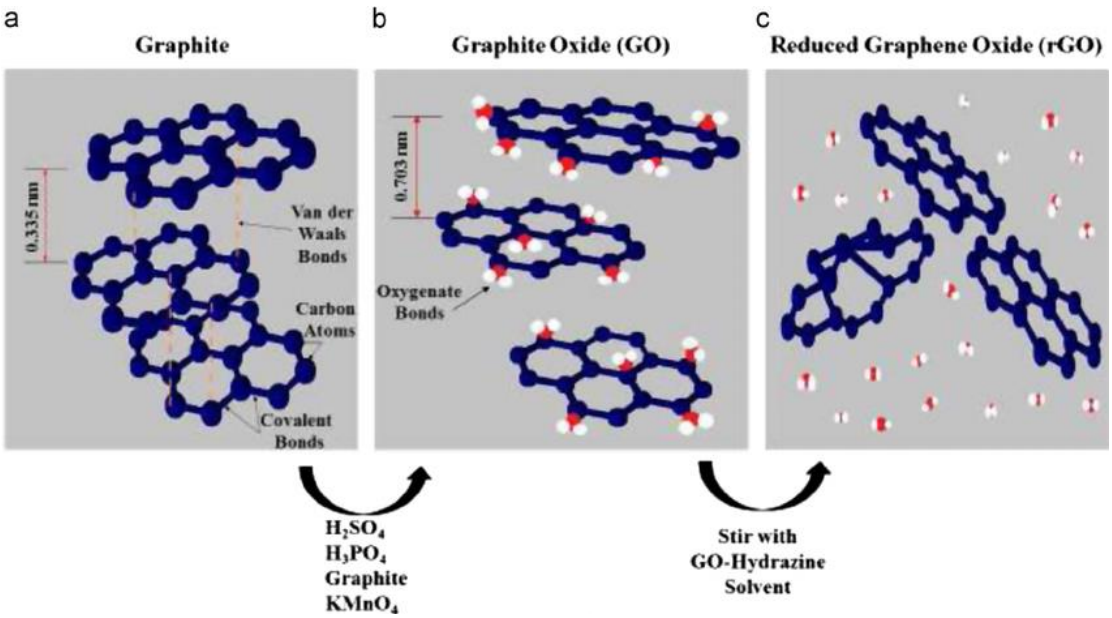

Figure 2.1 Schematic of rGO formation: (a) oxidation of graphite flakes (b) exfoliation of GO (c) received rGO after reduction. Reprint from ref [34].

The carbon slurry was made by blending self-made rGO powders with a diluted organic binder and depositing it on top of a carbon substrate. The binder solution

was first made with 7wt% of PVDF (Polyvinylidene difluoride) powder mixed into NMP (N-Methyl-2-pyrrolidone) and stirred for 12h before use. In making the carbon-based cathode, the carbon slurry was first blended together with rGO and organic binder solution with a weight ratio of 8:2 in a small nylon ball milling container and mixed for 2 mins to make sure everything is uniformly distributed. The slurry was then machinery coated on the top surface of the Carbon substrate. For this step, we choose to use the automatic thin film coater (MSK-AFA-3, MTI Co. shown in Figure 2.2) to obtain a relatively thinner and more uniform surface as for the capacity improvement while cycling. The carbon fiber substrate after coated is showing in Figure 2.1 (b). Finally, the coated carbon substrates were transferred to a vacuum oven and heated overnight at 80 °C. The large carbon cathode sheet was later cut into a 7/16-inch diameter circle and weighted before storing inside the glove box. The synthesis of Graphene Oxide (GO) and reduced Graphene Oxide (rGO) are shown below.

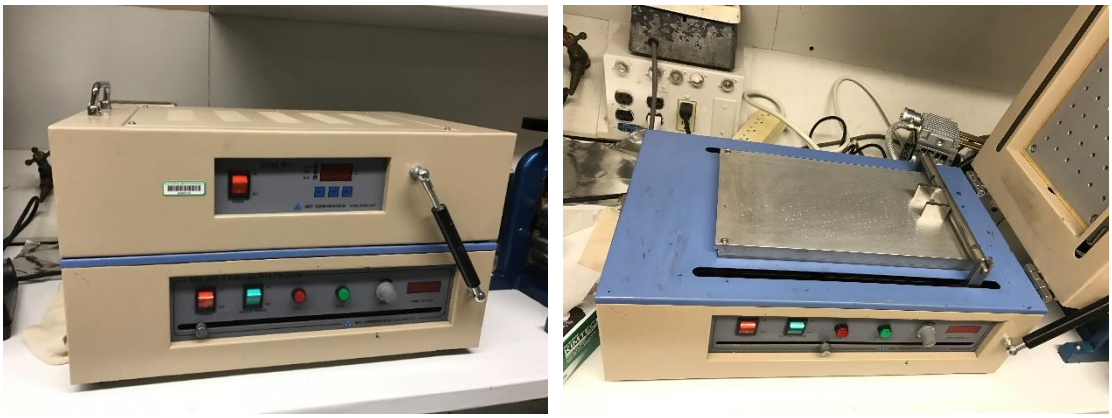

Figure 2.2 The MTI Co. automatic thin film coater applied for the thin film cathode coating for Li-O_2 battery.

2.1.1 Graphene Oxide Preparation

The GO was synthesized according to the modified Hummer's method [35, 36], 70ml of concentrated H_2SO_4 was poured slowly into an Erlenmeyer flask with 3.0g of flake Graphite powder (median 7-10 micron, 99.8% metal basis, Alfa Aesar) and 1.5g of $NaNO_3$. The mixture was cooled by using an ice bath at 0°C while stirring, and 9.0g $KMnO_4$ was added slowly into the mixture. The solution was kept under ice bath for 2 hours before removal. The mixture was then heated to 35°C and stir for 7 hours.

(a)

(b)

(c) (d)

Figure 2.3 synthesized Graphene Oxide portion (a) after taking out of the ice bath, (b) after pouring into ice water, (c) after centrifugation for the first separation, (d) the final received product.

An additional 9.0g of $KMnO_4$ was added to the mixture and kept at 35°C for another 12 hours. To further harvest the graphene oxide, the reaction mixture was poured on top of an ice-water solution (~400ml) containing 20ml of 30% H_2O_2. The precipitation was separated by centrifugation at 6500rpm for 10 mins and the supernatant was decanted. The GO obtained after centrifugation was washed 3 times in 400ml of 20% HCl followed by drying, and then washed again in 3 times of 200ml of methanol and dried in a vacuum oven at 60°C overnight. The pH tracked before first wash was nearly 0 and 4 before dried in an oven.

2.1.2 rGO synthesis and preparation

To further receive the actual cathode carbon material, which is reduced graphene

oxide, hydrazine hydrate was used as a reduction agent in order to exfoliate the GO to rGO [37-39]. The specific procedure is: graphene oxide (500mg) was added into a round flask bottle with 300ml of deionized water with a pH of 12 by LiOH. The inhomogeneous solution was then sonicated using the ultrasonic processor for at least 30 mins with an average frequency of 70Hz until it reaches an inhomogeneous brown color solution. Hydrazine hydrate (5ml, 15% in water) was then added to the solution and heated in an oil bath at 100°C for 20h with the water-refluxed condenser to achieve black colored precipitation from the solution. From fig 2.4, the rGO before reduction shows a uniformly black colored solution. However, after the solution has been heated for 20 hours the desired rGO completely precipitated to the bottom of the flask leaving a transparent supernatant which clearly shows the GO has been successfully exfoliated with the help of a reduction agent.

(a) (b)

Figure 2.4 the chemically synthesized rGO flakes (a) after ultrasound dispersion, (b) after final reduction.

The solution was then isolated by filtration and washed 3 times with 200ml of

deionized water and acetone until the pH becomes 7 of the filtrate solution. The collected particles from the filtration were then further dried in a vacuum oven at 80°C overnight.

2.2 Catalyst Synthesis and Characterization

2.2.1 Metallic $LiIr_3$ particles

It is barely reported in the literature regarding applications of $LiIr_3$ to scientific R&D since there is limited understanding of this intermetallic metal. One of the early structural investigation utilizing $LiIr_3$ was reported by H.C.Donkersloot and J.H.N.Van Vucht in 1976 [40], and this is possibly still the only report of this rare intermetallic among all scientists until now. Of course, no one has ever announced any detailed fabrication method related to the production of $LiIr_3$. However, in this research, with partial dated information, the $LiIr_3$ particles were successfully fabricated using a solid-state sintering technique from the mixture of Lithium and Iridium.

From the previous work [21, 41-43], Iridium metal powders have been demonstrated as the catalyst that effectively decreases the overpotentials during battery cycling and thus promoting higher cycles for the Li-O_2 battery. Lu et al [21] even raised the idea that Iridium powders will transform to $LiIr_3$ while discharging. The metastable intermediate discharge product, LiO_2, could be stabilized as major discharge products in favor of the epitaxy growth on top of $LiIr_3$, and as a result, drastically decrease the energy consumption during the Oxygen evolution reaction (OER). Based on the previous research done by J.H.N. Van Vucht et al [40, 44], the $LiIr_3$ could be fabricated according to the following chemical equation (11):

$$Li + 3Ir \rightarrow LiIr_3 \quad (11)$$

1.0 g of Ir (5.2 mmol, Aldrich powders 99.9 %) was first mixed with 14.44 mg of Li (1.73 mmol, thin foil) before being sealed in a Ta tube in Ar atmosphere glove box. An extra 20% of Li was later added to make $LiIr_3$ for fear of incomplete reaction. After that, The Ta tube with the crimped cap is taken out of the dry box and immediately sealed with an arc torch under Ar before further sealed in a quartz tube under vacuum.

Figure 2.5 (a) shows how the Ta tube that sealed in quartz tube looks like. As for solid state sintering, based on the Ir-Li Phase diagram proposed by J. Sangster and A. Pelson [45], The quartz tube that contains the mixture is then selected to heat to 800°C for 7 days in a furnace before furnace-cooled to room temperature. The synthesized Ir_3Li particles were analyzed in the SEM as shown in Fig 2.5 (b).

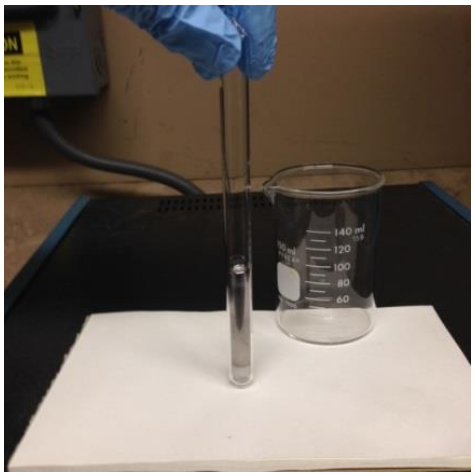

(a)

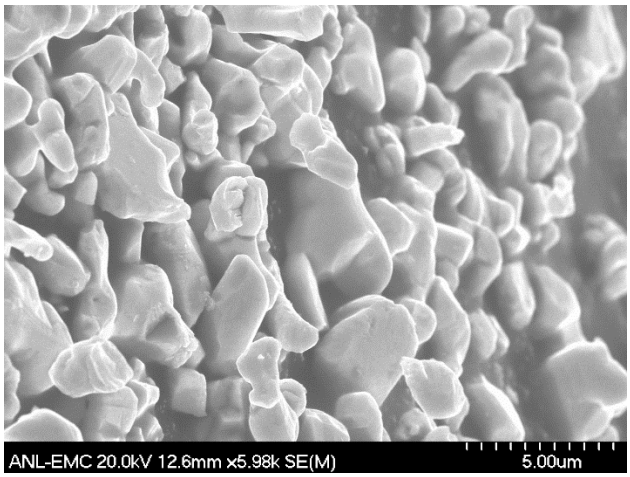

(b)

Figure 2.5 (a) Ta tube contain Iridium powders and Lithium after sealed in a quartz tube, (b) SEM image of the morphology of Ir_3Li particles after sintering.

2.2.2 Rhodium metal particles

Since the particle size of $LiIr_3$ was strongly dependent on the particle size of Ir powders, it was hard to achieve the nano-sized particles for better synthesis. In this research, another Rhodium nanoparticle catalyst that synthesized by a bottom-up technique was also selected and tested. The idea is to utilize the reduction agent like hydrazine to produce nano-sized Rhodium metal particles out from Rh^{3+} anion inside the $RhCl_3 \cdot xH_2O$ solution. At the same time, with the help of Hydrazine, the Graphene Oxide (GO) will also transform to reduce Graphene Oxide (rGO). This modified liquid phase reduction technique for Rh rGO is similar to preparation procedure for making rGO. The schematic illustration of making Rh rGO is shown in Fig 2.6.

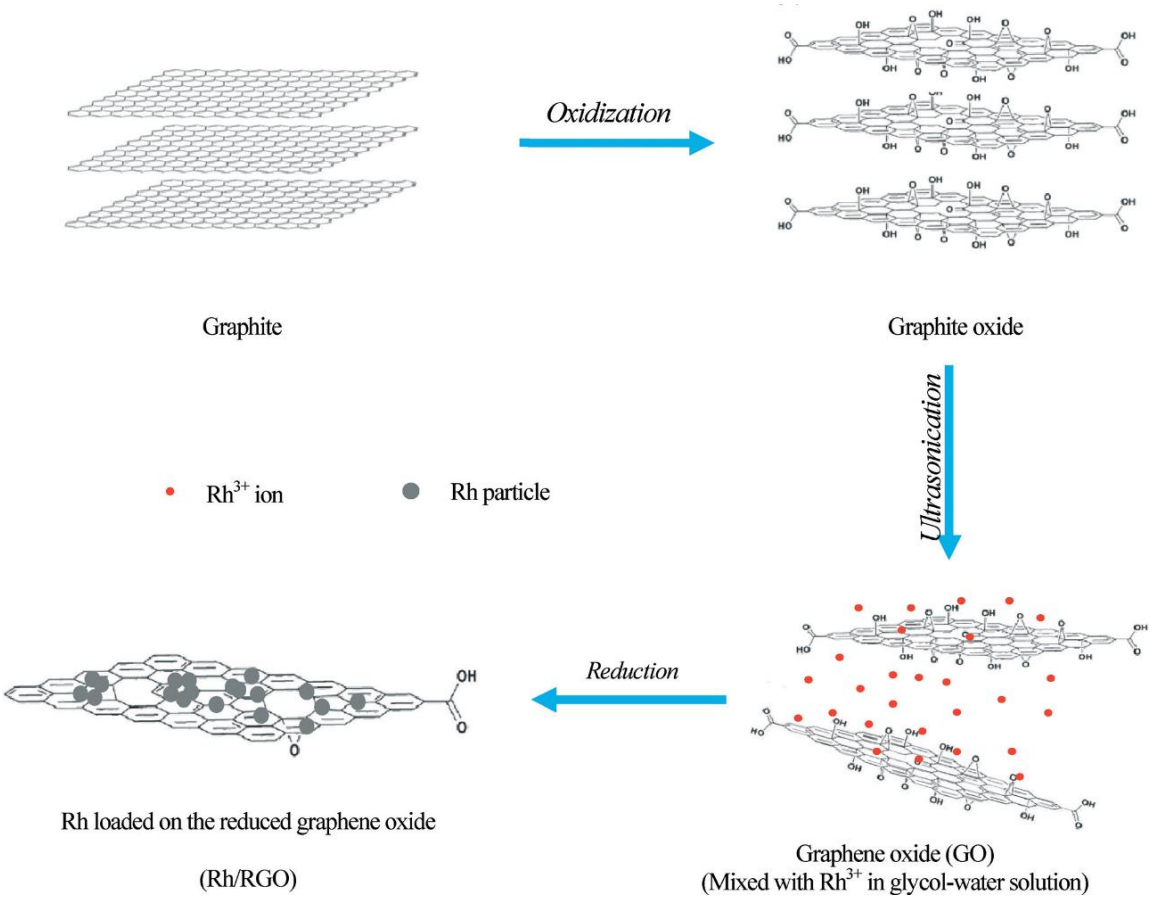

Figure 2.6 Illustration of the preparation process of the Rh/RGO catalyst. Reprint from ref [46].

To be more specific, At the beginning, 500mg GO was obtained by using the modified Hummers method [35]. In order to obtain the Nano sized Rh particles, $RhCl_3 \cdot xH_2O$ (Aldrich Chemical Co. Inc., x=3) was added to the portion as the donor of Rh anions before it was exfoliated by reduction agent. Despite that extra procedure, everything remains identical to the fabrication procedure of rGO. The final Rh rGO flakes after dispersion were collected and dried as shown in Figure 2.7.

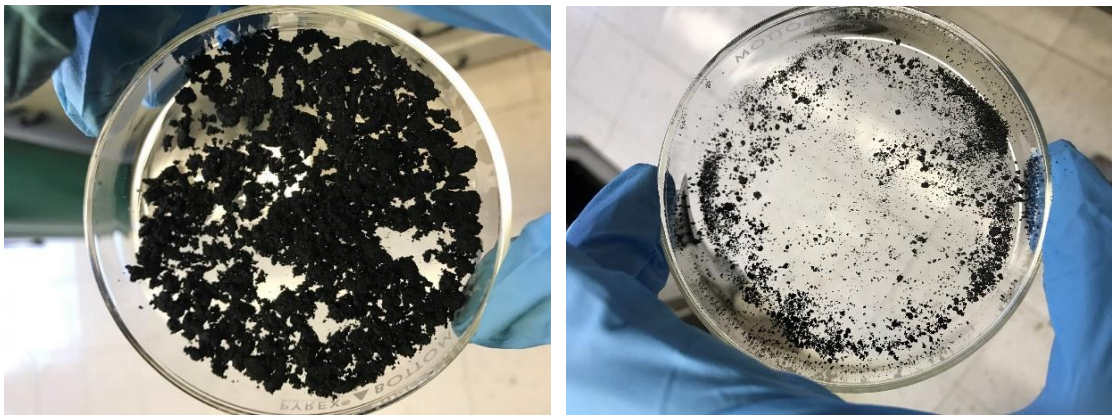

(a) (b)

Figure 2.7 the final Rh rGO particles (a) before drying and (b) after drying.

2.3 Battery cell assembling and testing

2.3.1 Swagelok cell

The Li-O_2 cell was assembled using a Swagelok cell packed with the battery components considered as the predominant part of the Li-O_2 Battery. It consists of a hollow nylon tube with 2 nuts (shown in Fig 2.8 a) fitting both sides of the tube in order to fasten the stainless steel current collector (shown in Fig 2.8 b). The materials made of tube and nuts from Swagelok company are chosen to be insulated nylon to avoid short circuits that could happen from battery sets inside the tube while battery testing (Fig 2.8 c shows all the parts of Swagelok cell in sequence before assembling, whereas Fig 2.8 d is a picture of Swagelok cell after assembly and ready to seal with Oxygen). The Swagelok cell also contains two sets of nylon ferrule with a diameter of 1/2 inch with the purpose of sealing the current collectors in case of poor contact of the battery parts inside Swagelok cell. Both sides of current collectors were designed and further fabricated at Argonne National Lab. The anode side was designed to be a

stainless-steel cylinder with 1/2 inch and 35mm length. One side was polished for direct in contact with anode Li metal whereas another side was machined with a screw hole to clamp with a current clamp. It is easier when switch to the cathode side of the collector, also a cylinder-shaped but the hollow tube that made of aluminum was machined to provide sufficient oxygen since oxygen is in direct contact with carbon-based air permeable cathode inside the glass chamber.

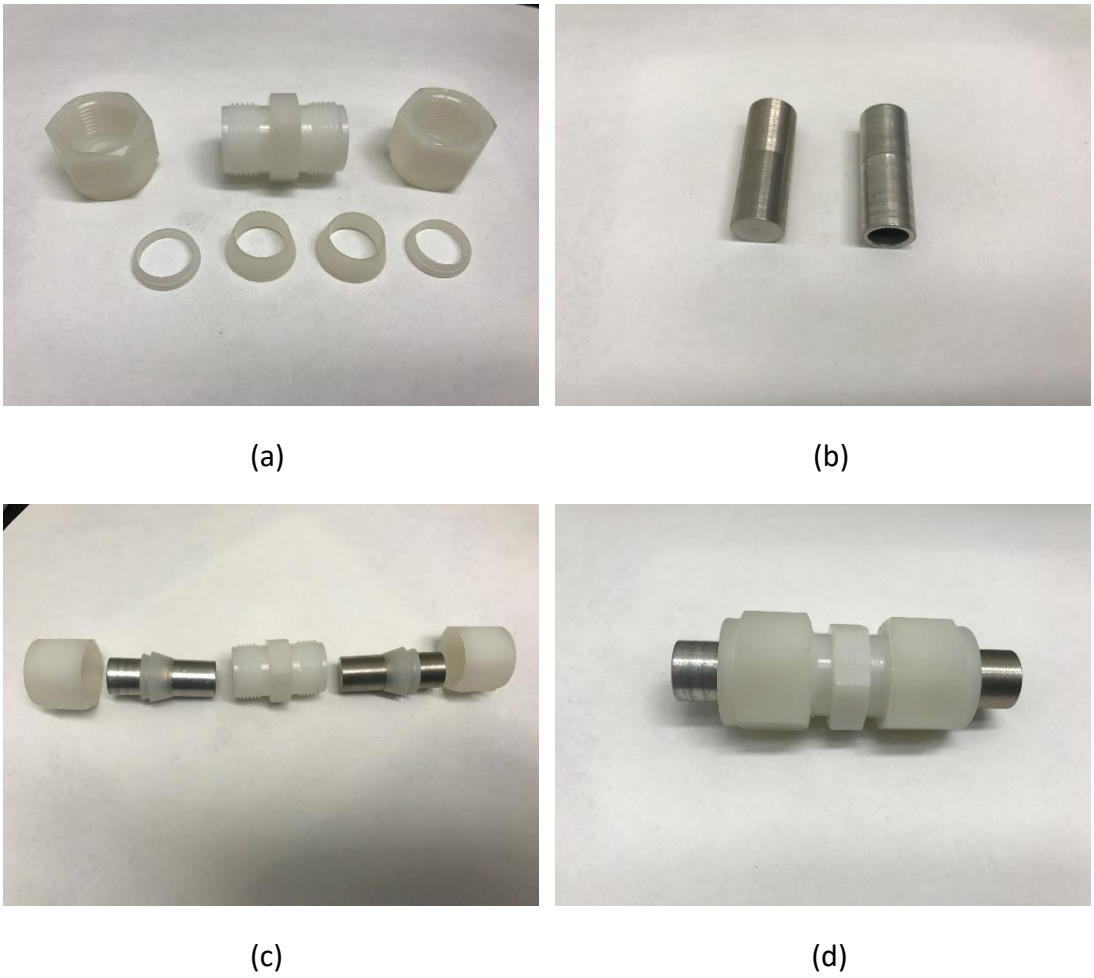

(a) (b)

(c) (d)

Figure 2.8 Photo of the (a) Swagelok part. (b) Stainless steel current collector. (c) Schematic of cell assembly sequence. (d) Fully packed Li-O_2 Swagelok cell.

When it comes to the battery component inside the Swagelok cell, it normally consists of a piece of lithium metal foil, a cellguard glass fiber separator that wetted

with certain electrolyte and a carbon-based catalyzed cathode. An aluminum mesh has been used to attach to the back of the cathode and the hollow current collector in case of battery deformation during the assembly. Last, the two ends of the battery electrode were attached to the current collector and sealed with Swagelok cell components. The schematic is shown below in Fig 2.9. The size of Swagelok cell and battery set are designed to be 1/2 inch except for both electrode and aluminum mesh, which is only 7/16 inch, to avoid the possibility of short circuit that happens on the edge of the electrode while assembling.

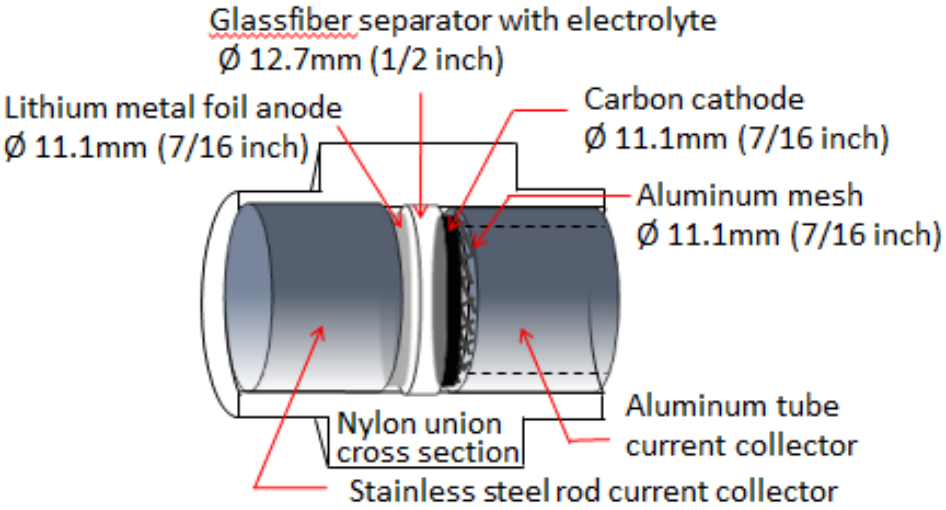

Figure 2.9 the schematic draft of a battery assembly inside the Swagelok cell. Reprint from ref [11].

When it comes to battery assembling, the central nylon union and the cathode side current collection will first tighten up as the bed for the battery set. The aluminum mesh, electrode and separator will then place inside the nylon unit respectively. Before putting the anode collector on top and finally sealed the Swagelok cell, the selected electrolyte will be dropped on top of the separator with pipet until it's fully wetted, that will approximately be 0.3 to 0.5ml (~6 to 10 drops of the electrolyte

with pipet). After screwing up both sides of the nylon nut, a Li-O_2 battery placed inside a Swagelok cell

2.3.2 Oxygen filled glass chamber

Testing the battery cell is under an Oxygen atmosphere performed by utilizing a gas-tight glass chamber which consists of two gas flow valves and a set of the current collector to seal the battery pack inside the chamber, as shown in Fig 2.10 (a). To be more exact, for the top cap part, two conductive clamps with wires are supposed to connect two ends of the Swagelok cell. Another side of the wires was then exposed outside through the lid to connect with the cycling tester. The Swagelok cell and two separate wires complete the whole battery circuit. The bottom part of the glass capsule is simply designed to contain the whole Swagelok cell and the current collector. The top and bottom glass part was then gear together and sealed by laboratory grease as well as a large clip to avoid gas leaking. In order to purge the oxygen into the glass chamber, two plastic gas valve with rubber rings was placed on both ends of the glass chamber. By twisting this two plastic valves, the inner cellular can be either sealed or perforated for gas purging. The cell after assembling was shown in Fig 2.10 (b).

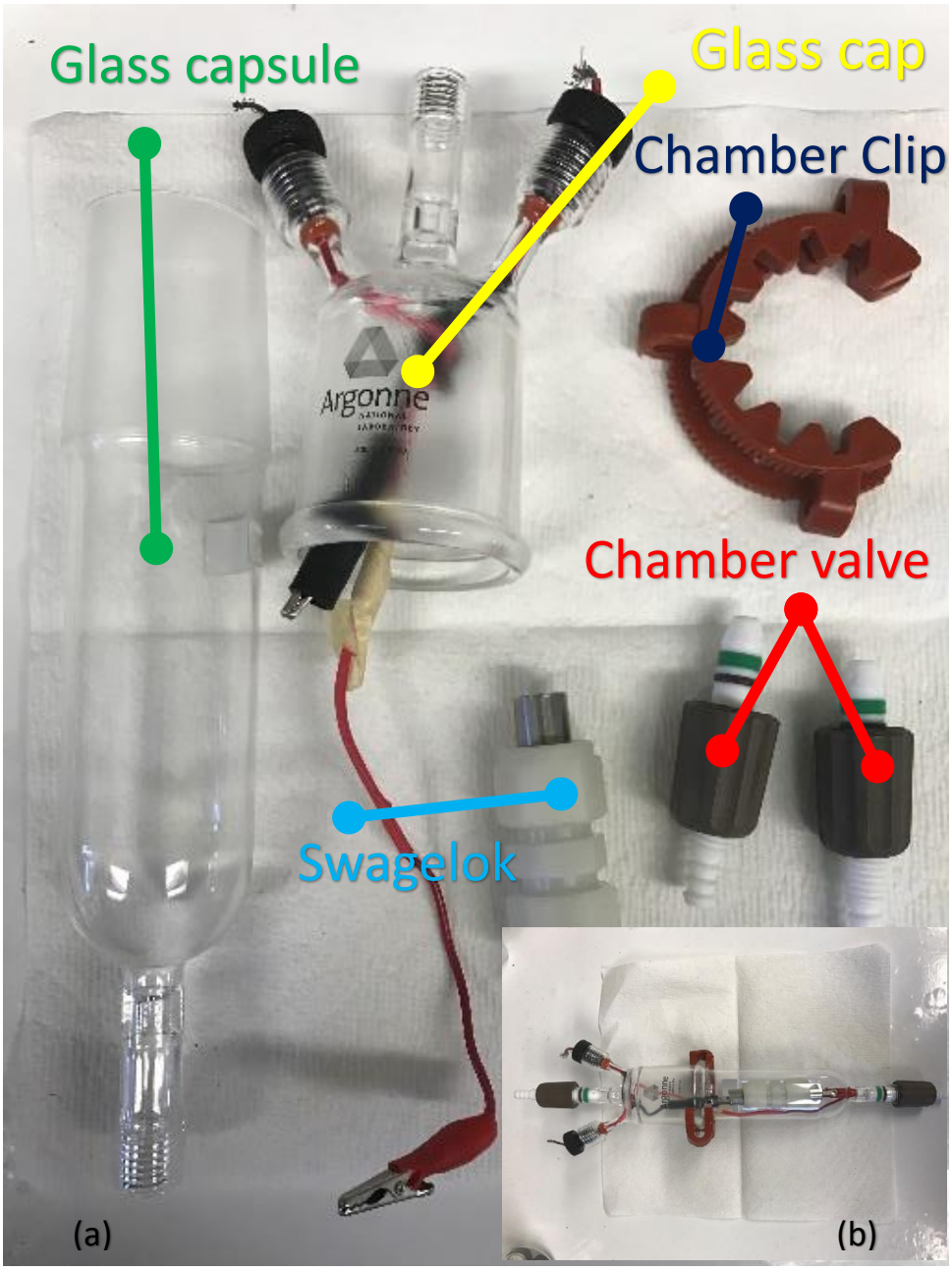

Figure 2.10 (a) All the cell component needed from a Li-O_2 cell. (b) A completed after-assemble Li-O_2 cell.

To avoid the gas contamination as well as water content from air ambient, all the battery assembly procedures were completed in an Argon ambient MBRAUN glove box with H_2O and O_2 level both lower than 0.1 ppm. After the battery was assembled, it will transfer out from the glove box with the valve closed and immediately purged

with highly purified oxygen for 30 mins with a constant airflow rate before the test. As shown in Fig 2.11, the oxygen coming from the gas tank goes in and out through two pipes that were connected to the tunable airflow valve on the glass chamber.

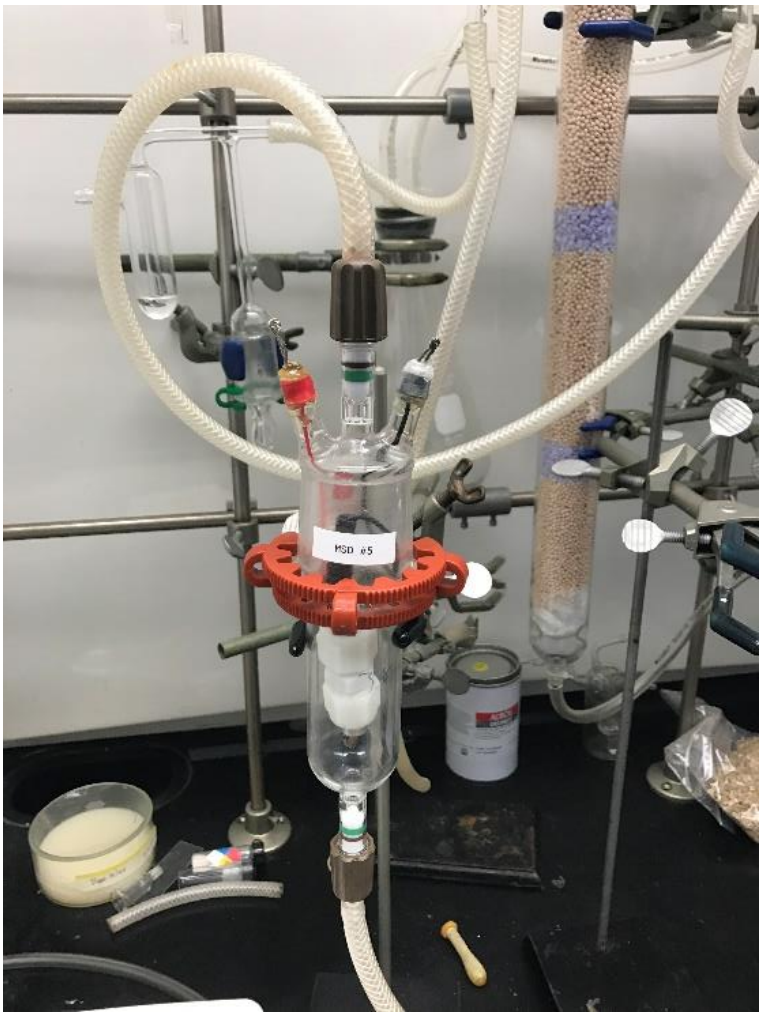

Figure 2.11 shows the Oxygen purging process. The high purity oxygen gas flows through the bottom to the top port inside a glass chamber sealing with a Swagelok Li-O_2 battery cell.

After 30mins of high purity oxygen gas purging, the Argon gas now is considered completely replaced, and the battery cell is now ready for battery cycling test by using the Maccor® battery testing machine shown in Fig 2.12.

(a) (b)

Figure 2.12 (a) a Maccor® S4000 battery cycler used for cell performance test, (b) picture took from the inside of battery testing hood. The battery chamber is stacked on the shelf and connected by two current collecting clamps.

3. Design Improvements to Enhance Li-O_2 Battery Performance

3.1 Selection of the Cathode

A variety of materials have been selected as cathode substrates based on the properties of high air permeability, conductivity, and oxidation resistance. H. Wang et al [47] investigated the carbon-based cathode with aprotic electrolyte and concluded that the cathode passivation is the predominant reason responsible for the low cyclability of the battery since it becomes insulated due to the accumulation of discharge products. Although the cathode is not permanently damaged, the importance of cathode substrate fabrication is yet indisputable.

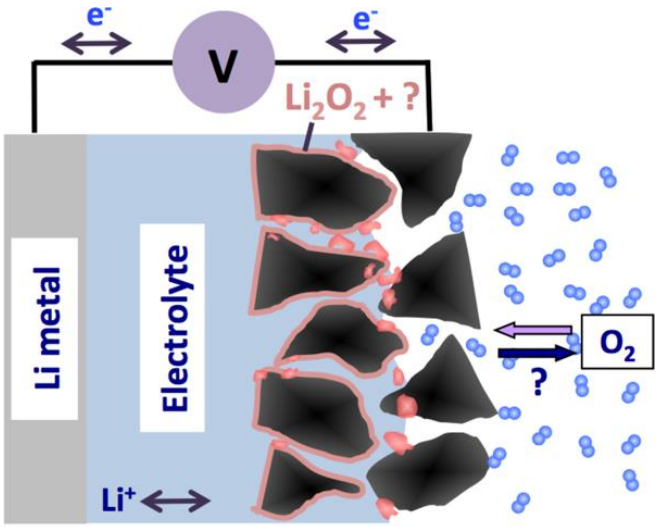

Figure 3.1 Schematic illustrating the electrochemical reaction in air at the cathode for a Li-O_2 battery. Reprint from ref [28].

As mentioned earlier, the cathode is made by coating a selected conductive slurry on

certain porous holder (or current collector) in order to support the oxygen while ORR. Fig 3.1 shows the schematic of how the cathodic reaction happens in the Li-O_2 battery. In order to improve the cathode performance, this investigation has focused on two different aspects; the cathode materials and the cathode holder.

3.1.1 Selection of Cathode Materials

There are various types of actual cathodes reported being applicable for Li-O_2 cells, like TiC-based [27] or nano-porous gold [48]. Carbon has become the most selected materials for the air cathode for its lightweight, controllable size and morphology and high conductivity [36, 38]. Besides, carbon is also the simplest and cheapest materials among all the competitors. There has been a uncountable number of carbon-based cathodes that have been investigated, like conductive graphitized carbon [49], Super P [26] or activated carbon [50]. All of them have been separately investigated by previous researchers and has been justified as functional for cathode materials of Li-O_2 cells as a factor of low overpotentials and better cyclabilities [51]. The commonly used carbon for air cathode in the Li-O_2 battery is believed to be the reduced Graphene Oxide (rGO) because of its excellent in-plane mechanical, structural, thermal, and electrical properties [43, 52], which is considered to favor the growth of the discharge product due to its high surface area.

As mentioned earlier, pore-clogging and cathode insulation are responsible for most of the battery damage and low cyclability. Furthermore, the carbon surface is relatively amenable to some reduced oxygen species that eventually causes the carbon corrosion while battery cycling. Irreversible side-products (e.g. Li_2CO_3) will form on the SEI layer, limiting the cycle life of Li–O_2 batteries. Thus, the morphology of carbon cathode is an inevitable factor in choosing materials. The porous structure does not only conduct electrons but it also accommodates the solid-state Li

deposition that enables the diffusion of the electrolyte and oxygen [43].

Several methods have been developed by researchers to prevent or decrease carbon corrosion and the accumulation of side-products. P. Bruce et al. [53] reported that by HNO_3 oxygenated carbon was more unstable than the one heat treated in an H_2/Ar atmosphere in Li-O_2 batteries. Y. Shao-horn et al. [54] have shown that carbon materials with a low number of functional groups exhibited better stability. It is barely reachable to completely cover the surface area of the cathode with carbon, so tuning surface heteroatoms (e.g. oxygen) through adjusting the surface chemistry of carbon is a feasible idea for enhancing the carbon surface stability [37, 52]. Recently, W. Zhou et al. [43] also demonstrated that the graphene cathode with Iridium catalyst displayed preferable cycling performance in Li-O_2 batteries. Other than that, Gittleson et al. [55] also concluded that the rGO is the wisest choice when encountering large-scale industrial applications such as energy storage since the easy accessibility of large quantity fabrication.

In this thesis, the synthesized exfoliated graphene oxide is the chosen cathode substrate embedded with selected catalysts. However, the performance comparison of rGO and Super P carbon will also be presented.

3.1.2 Synthesized rGO characterization

In this investigation, the method proposed by M. Daniela [35] has been followed because it is considered to be more productive than the modified Hummers method. However, a lot of concentrated H_2SO_4 and H_3PO_4 (400ml in total compared to 70ml from modified Hummer's method with the same quantity of graphite needed) are involved in the oxidation of carbon, which makes the work more complicated after the oxidation. It was observed while washing the received graphene oxide with

filtration, the high viscosity of graphene flask (shown in Fig 3.2 a) immediately clogged the pore of the filter paper. Another issue was that during centrifugation, as an alternative way to wash the GO out, the solid deposits are extremely hard to deacidify with such high volume of concentrated acid. The pH of the whole portion still remained at 1 after washing five times in water and methanol. As a result, the received GO never dry off since the existence remaining non-vaporable acid.

(a)

(b)

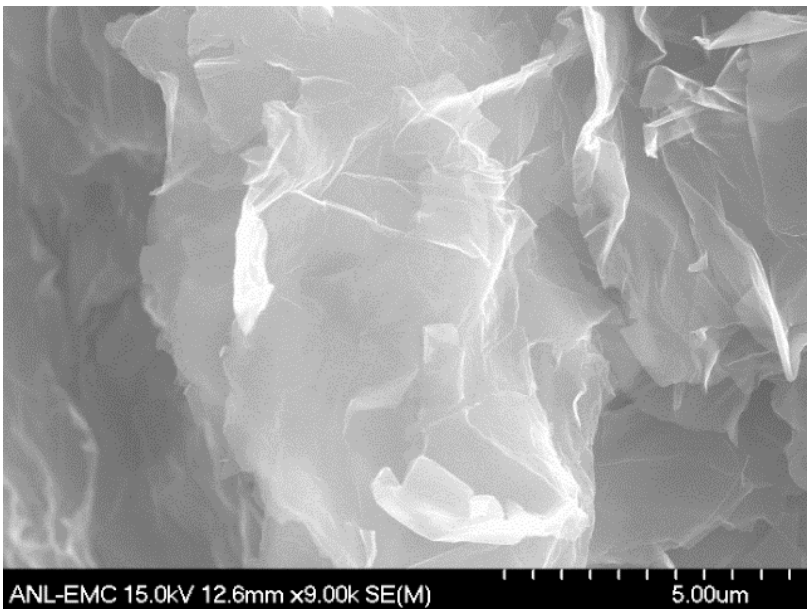

(c)

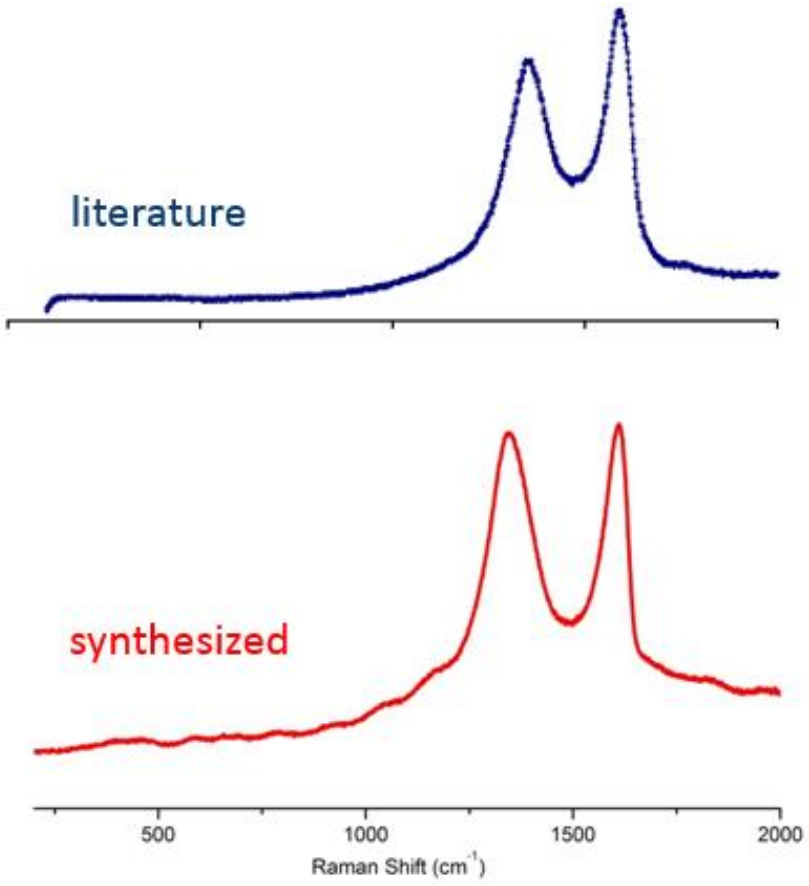

(d)

Figure 3.2 oxidized graphene oxide with (a) improved method, (b) modified Hummer's method, (c) SEM image of synthesized GO after drying, (d) Raman spectra comparison of GO from synthesized and literature.

Then, the idea for making GO shifted back to modified Hummers method [35] that has been chosen by various of other researchers [21, 37, 46, 54, 56, 57]. Besides, the size distribution of graphite flake is controlled to be as small as 40 microns to avoid clogging. As shown in Fig 3.2 (b), the mixture that received this time was better in mobility and way much easier to wash to a pH of 7. In conclusion, although the more productive improved method is promising, the following procedures to wash it out are much more complicated than simply choosing the modified Hummer's method, the latter is eventually decided to utilize for synthesizing GO in this research.

The synthesized GO are characterized by SEM and Raman, the results are presented in Fig 3.2 (c) and (d). SEM image shows the graphite has been oxidized to a much larger and irregular spacing yet retains the layer structure which does not process the morphology of stacked layer like as graphite. Instead of that, the single sheet graphene-like sheet is predominant, which justified the existence of transformation from graphite to Graphene oxide. Furthermore, Raman spectra show both G and D bond peaks for carbon that lie at around 1560 and 1360 cm^{-1} are observed from self-fabricated GO, which is identical to the results observed by other researchers [38]. Both results verified that the Graphene oxide has been successfully fabricated with the modified Hummer's method mentioned in chapter 2.

When it comes to the reduction of Graphene oxide, there is variety reduction idea reported to exfoliate the Graphene Oxide to Reduced Graphene Oxide to achieve the further improvement in topography and conductivity to a more desirable single-sheet graphene structure that make it feasible for not only battery but other application fields. Among all reduction methods, three of them are winning the chair, which is a chemical, hydrothermal and thermal reduction [21, 37, 38]. The thermal reduction method requires certain treatment as well as the heating temperature of 1100°C, which is hard to manage. Thus, in here we just choose the first 2 methods as a comparison for reduction process for Graphene Oxide.

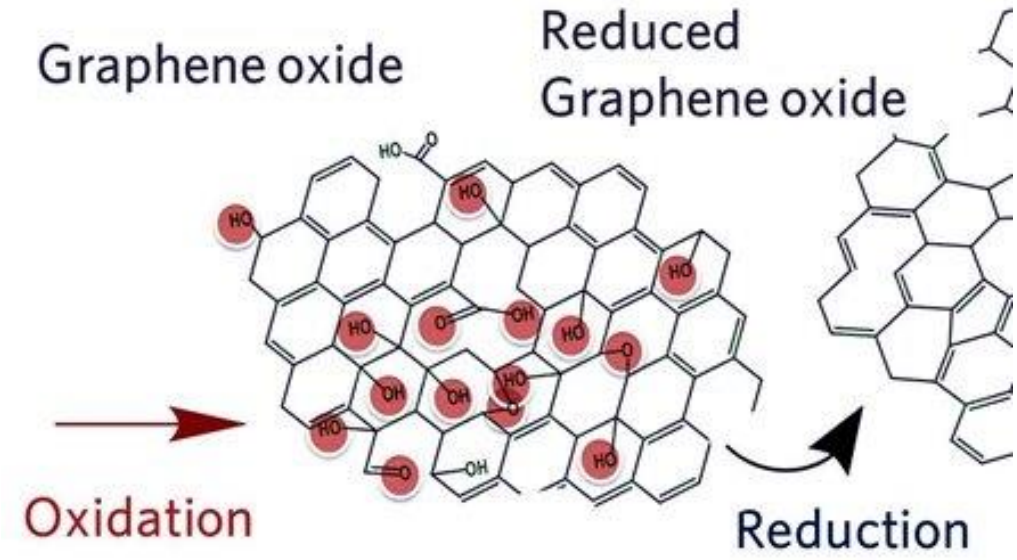

Figure 3.3 Schematic shows how the microstructure shift happened while reduction of Graphene oxide. The red marked circle is epoxy bridges, hydroxyl groups and pairwise carboxyl groups formed by oxidation of graphite. Reprint from ref [55].

The reduced graphene oxide with a simply modified method for from literature [21, 37] is shown in Fig 3.3 as a comparison. Other than reduction procedure recorded in literature, we do an extra step of pH balancing for both of the treatment to keep the pH at 11 in order to keep the dispersion stability [58]. For the hydrothermal method, the GO was first ultrasound for 30 minutes with deionized water, the pH of the mixture was then tuned to 13 before captured into a cylinder-shaped ceramic container (shown in Fig 3.4) that sealed inside a stainless container as the hydrothermal reactor. The whole set will then transfer into a furnace and heated for 12 hours at 180°C before furnace cooling.

(a) (b) (c)

Figure 3.4 (a) and (b) shows the ceramic container and the stainless holder for the hydrothermal kit that used while reduction of GO; (c) the received rGO appears as aggregated cylinder-shaped structure.

Different from what we have seen from chemical reduction with hydrazine hydrate (detailed in Chapter 2, fig 2.3), which is finely dispersed in a liquid solvent, the final product of rGO after the hydrothermal process is always left as a condensed cylinder-shaped aggregation. The hypothesis for this phenomenon is the high-pressure circumstance inside the sealed ceramic container while heating. A reduction of graphene oxide is always accompanied with CO_2 releasement caused by the heating process damages the structure of the graphene platelets as the pressure between builds up. The high gas pressure inside the solvent eventually formed an extrusion force that squeezes the dispersed rGO together because of container-shaped aggregation. Other than that, high-temperature treatment also causes a substantial reduction in the mass of the GO (approximately 30%wt from the original), creating imperfections and vacancies, and potentially also influencing the mechanical strength of the rGO produced (Presented in Fig 3.3).

While the aggregation is formed, it is highly possible that the dispersed graphene flakes will stack together instead of exfoliated as desired due to the external forces. The SEM images of the morphology of fabricated rGO then justified the correctness

of the hypothesis presented in Fig 3.5. While the rGO harvested with chemical reduction method appears as graphene sheet layer in fig 3.5 (a), the hydrothermal method fabricated rGO shows the morphology of bulk carbon fragment without any classical features of graphene at all (fig 3.5 b). The pH after hydrothermal was tested to be in the range of 7, which is due to the reduction of GO as mentioned. However, data from Raman spectroscopy (Fig 3.5 c) indicate that spectra from both reduction techniques possess a sharp G and D bond carbon peak, which is identical to the rGO spectra that provided from literature, this result means the reduction process works for both hydrothermal and chemical methods and the achieving products are identified as reduced Graphene Oxide (rGO). However, the actual quality of received rGO varies a lot with their qualities. Obviously, the morphology of rGO received by hydrothermal method does not fit the criteria of high surface area and low packing density of graphene sheets, which leads it unsuitable for energy storage or a related application.

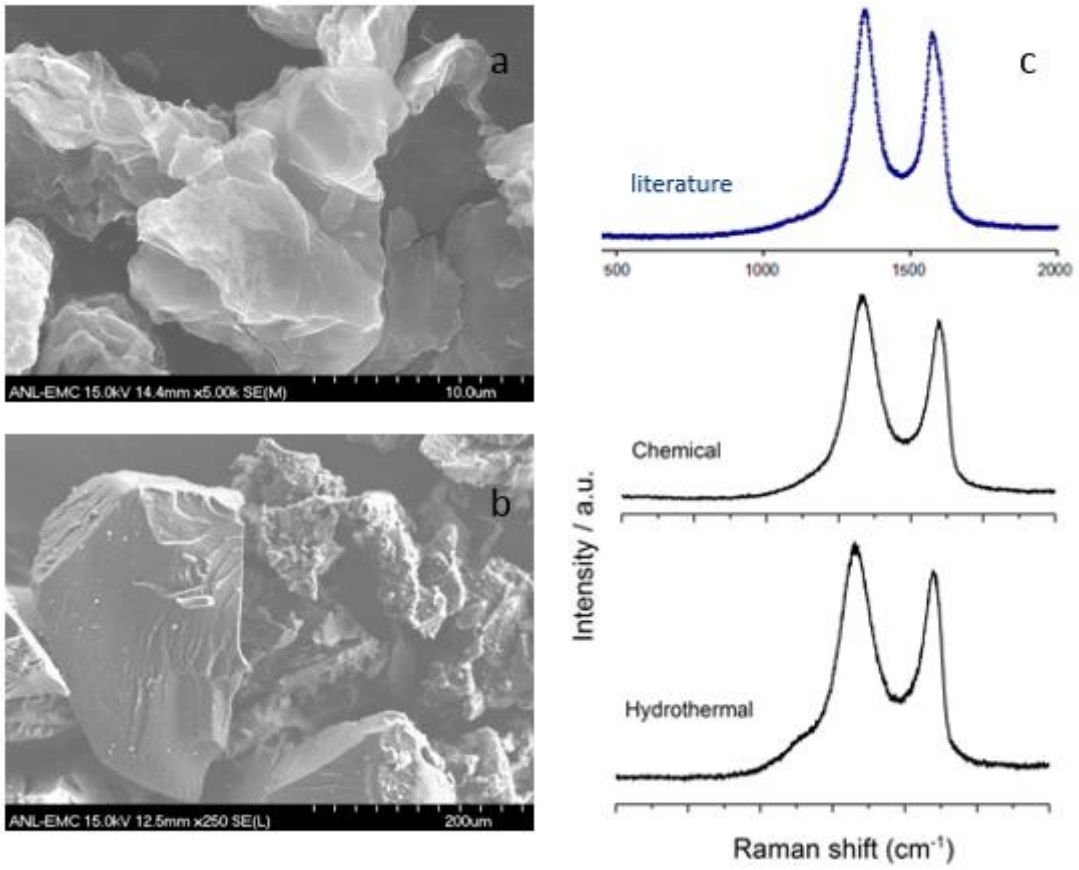

Figure 3.5 as received reduced graphene oxide with (a) hydrothermal method, (b) chemical reduction method, (c) Raman spectra comparison of rGO with literature.

In conclusion, after listed synthesis and characterization, the reduced Graphene Oxide fabricated by chemical reduction method is selected for the cathode materials in terms of the high conductivity and surface area as well as capacity of large-scale engineering application. One thing should mention here is that the reduction agent we choose in this work is hydrazine hydrate, which is also the predominant choice for most of the researchers. Yet hydrazine hydrate is highly toxic, besides there is people suggested that the possibility of remaining C-N groups are non-negligible [38]. The alternative reduction agents are also investigated by researchers, such as Sodium Borohydride ($NaBH_4$) [58]. However, the morphology of the synthesized rGO is not

provided, so we would not know whether it is applicable in this application. On the other hand, the hydrazine is reported to be more efficient under alkaline circumstances. There might be a further investigation regard to this comparison, yet hydrazine hydrate is still the only reduction agent selected for fabrication.

3.1.3 Selection of carbon fiber substrate

Then it comes to carbon fiber substrate. Although P. Bruth et al [27] announced that Carbon decomposes during oxidation of Li_2O_2 on charging above 3 V and this could positively initiate the electrolyte to decompose while redox, it eventually announced unsuitable for aprotic Li-O_2 cells.

However, it is still the most widely used cathode holders for most of the Li-O_2 battery research [21, 43, 53, 54] regards to its remarkable ability of manageable surface morphology and porosity as well as high conductivity, which are assignable to cathode mechanisms for Li-O_2 battery.

Table 3.1 data sheet for two selected gas diffusion layer as electrode substrate

Properties	Fuelcell® GDL			SIGRACET® GDL	
	unit	TGP-090	TGP-120	unit	GDL 35BC
Thickness	mm	0.28	0.37	mm	0.325
Porosity	%	78	78	%	80
Gas permeability	ml·mm	1700	1500	$cm^3/(cm^2 \cdot s)$	1.5+/-1.0
Electrical resistivity	mΩcm	80	80	mΩcm	<19.5

Again, compared to stainless steel current collector reported and utilized by P. Bruth [27], a carbon fiber cathode holder can provide the maximum surface area with capable air permeability; instead of a mesh structure cathode, a porous solid shaped cathode can definitely provide more surface holder area for cathode material, and as a result favorable for the continuous growth of discharge product. Table 3.1 shows the material properties of two selected types of carbon fiber holder. One can tell from that table that they are similar in thickness and porosity, whereas the conductivity and air permeability varies a lot. The difference in properties can be explained with the SEM images taken from the surface of the pristine surface of both carbon holder that shown in Fig 3.6.

Initial cathode preparation involves only the regular type fuel cell brand Toray carbon paper. The morphology of the surface is showing in Fig 3.6 (a). It consists of PAN carbon fiber with 3 to 10 microns in diameter. The fiber itself possesses high tensile strength and electrochemical corrosion resistivity. All the fiber is tightly connected with carbon; the ultimate airflow permeability makes it highly feasible for gas diffusion cathode application. However, the big porous surface makes the holder extremely hard to hold the carbon slurries remain in contact with an electrolyte-wetted separator. In another word, the porous structure formed with simply connection with carbon fibers can be few hundred microns in diameter, yet the size distribution of the cathode slurry carbon materials is just around 5 micron, most of the carbon slurry will be drifted inside the pole instead of binding on top of the surface (showed in Fig 3.6 (b). Then, there are two problems come with it as the demand of being holders for the cathode. First, an unknown amount of cathode carbon particles will drop inside the pore and as a result, there will be insufficient actual cathodes that in contact with the separator, which is the only component inside the battery that soaked with electrolyte, the battery will expectantly run with shorter lifetime due to poor circuit connection between two electrodes. Second, the

capacity for the Li-O_2 battery is always calculated with the unit of $mAhg^{-1}$ [4], which means the current density is always calculated as mAg^{-1} instead of $mAcm^{-2}$. In this case, it is inevitable to achieve a desirable high capacity of a Li-O_2 cell with less weight of cathode loading. Literally, the lower the actual cathode loading is, the higher the capacity will be with the other parameters remains identical.

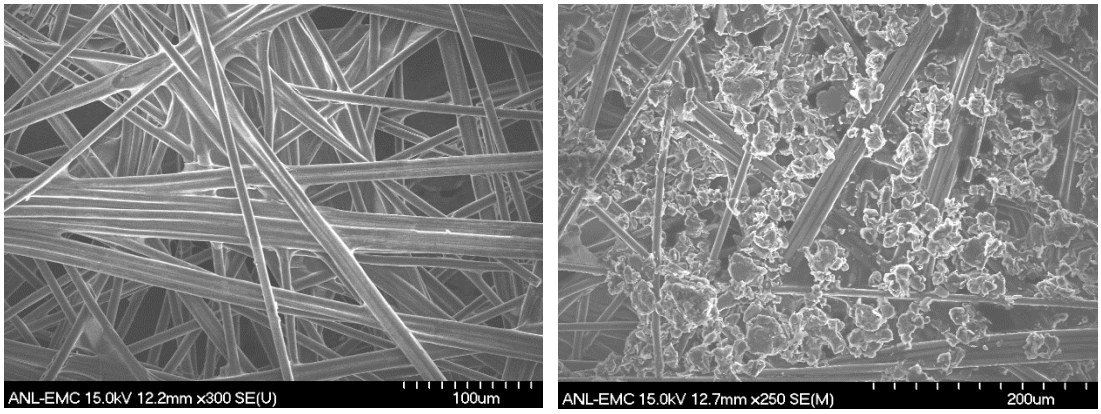

(a) (b)

Figure 3.6 SEM image of the (a) fuelcell 090 carbon fiber GDL, (b) an rGO coated 090 carbon fiber cathodes.

The hypothesis has been justified as existing for a glass fiber carbon holder as the SEM image showed in Fig 3.6 (b). From that image took on the surface of the electrode, one can easily tell that the carbon slurry particle is submerged in those giant mesh holes that formed by carbon fiber, so it is difficult to tell the actual surface area of a cathode while involving in a redox reaction. Besides, as mentioned before, the actual loading of the cathode is always weighted to be higher than 2mg. As a result, the capacity is restrained to be less than 500mAh/g even with a high current density.

After the awareness of this case, the SIGRACET brand MPL pre-coated carbon

diffusion layer was then come to utilization. Instead of massive scale hole that spread all over the place for carbon fiber paper, the GDL 35BC got surface enhanced with pre-coated with non-stick PTFE (Polytetrafluoroethylene, the best-known name of PTFE-based formulas is called the well-known “Teflon”) to form a hydrophobic surface to avoid corrosion. Other than that, another layer of the unique carbon-based microporous layer (MPL) was also utilized as the function of the gas diffusive membrane as well as a functional holder for surface materials on top of it. As the given SEM picture in fig 3.7 (a), the porous surface structure of the microporous layer (MPL) was observed, the particle size of the components of the layer is believed to be Nano-size. Compare to the diameter of few hundred microns of porous structure for the Toray carbon paper, a GDL 35BC carbon paper only processes the diameter of less than one micron for the pore that finely distributed on the microporous layer (MPL). Frankly speaking, the air permeability of the surface would be lower compared to the regular carbon fiber since the diameter of the hole decreased a few magnitudes, yet all the other parameters are improved with the help of the double-layer coating.

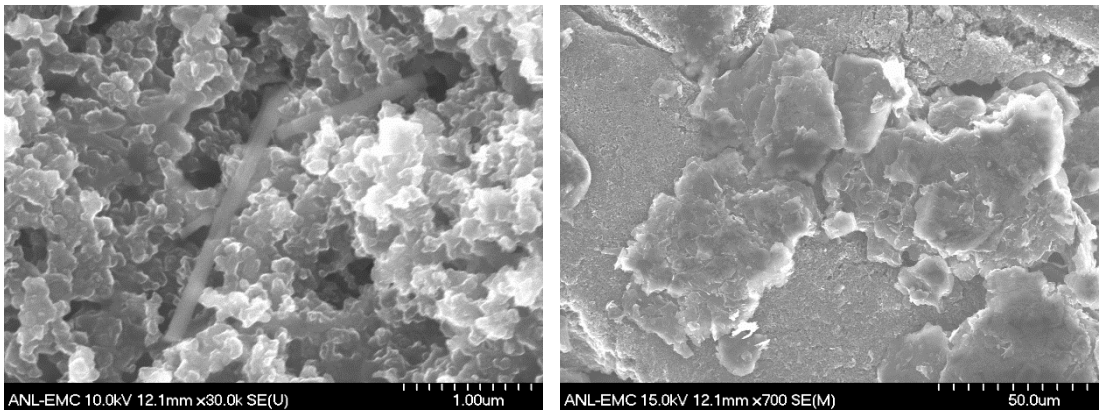

(a) (b)

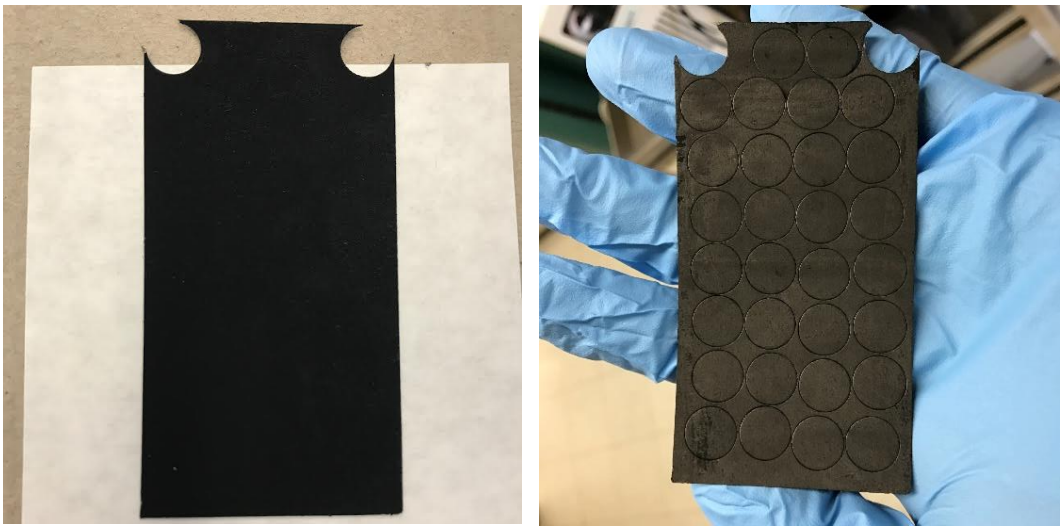

(c) (d)

Figure 3.7 SEM image of the (a) Sigracet brand 35BC GDL, (b) an rGO coated MPL treated carbon cathode; (c) the picture took from pristine Sigracet® GDL carbon paper, and (d) coated carbon paper cathode after drying and punching.

Besides that, in favor of the Nanoscale coating surface, the downgrade size scale, as well as distribution of the top surface, makes it more favorable for being the bed of the carbon slurry. As mentioned before, most of the graphene oxide carbon that fabricated as a cathode are believed to have the size no less than a micron, in this case, from the morphology pictures showed in fig 3.7 (b), the problem regards carbon holder with enmeshed slurry could simply fix with GDL carbon paper. As a result, we could efficiently use the same technique (Chapter 2, cathode fabrication part) to make cathode with the actual loading from 0.15mg to 1mg instead of over 2mg with Toray carbon paper. As the actual weight of carbon cathode gets lower, the new Li-O_2 battery can run with at least tripled capacity with all identical condition compared to the cells with Toray carbon cathode. The pristine selected Sigracet® GDL carbon paper is shown in Fig 3.7 (c) and the finally received self-fabricated cathode after coating is shown in Fig 3.7 (d).

3.2 Selection of electrolyte

As reported by Yamamoto et al. [8], the electrolyte is what distinguishes the nonaqueous (aprotic) lithium-air battery from its aqueous sibling. It must possess a wide range of attributes, as listed in Table 3.1. In particular, Yamamoto et al. [8] also emphasized that to achieve the reversible formation/decomposition of Li_2O_2 at the cathode on discharge/charge brings the major challenge to the electrolyte. Selecting electrolytes that permit the efficient and highly reversible formation of Li_2O_2 at the cathode is critical for the aprotic Li-O_2 battery present.

Table 3.2 Requirements on electrolytes for the nonaqueous Li–O_2 battery. Reprint from ref [8].

conductivity	Sufficiently high for the anticipated rate capability
Stability	Within potential window used on discharge and charge
	In contact with O_2 and its reduced species on discharge
	In contact with Li_2O_2 and its intermediates on charge
	In contact with the anode or SEI formed on the anode
Low volatility	To minimize evaporation at the porous O_2 cathode
O_2 solubility and diffusivity	To ensure adequate rate of mass transport to the cathode
Able to wet the electrode surfaces	
Promotes some solubility of Li_2O_2	Interaction with intermediates for high rate and packing density of Li_2O_2
Safety, low cost and toxicity	

Most of the case, the electrolyte reported in Li-O_2 battery is TEGDME (Tetraglyme),

DME [59] (Dimethoxymethane) or DC with the lithium salt such as $LiCF_3SO_3$ (Lithium triflate) or LiTFSi (lithium bistrifluoromethanesulfonamide) [8, 14, 17, 19, 21, 25, 41, 59-61]. Among all the kind of electrolyte solvent, the TEGDME are commonly chosen in terms of its chemical structure (four ether chains ended with two methyls, shown in Figure 3.8 a) which are believed to be durable under multiple oxidations while battery cycling.

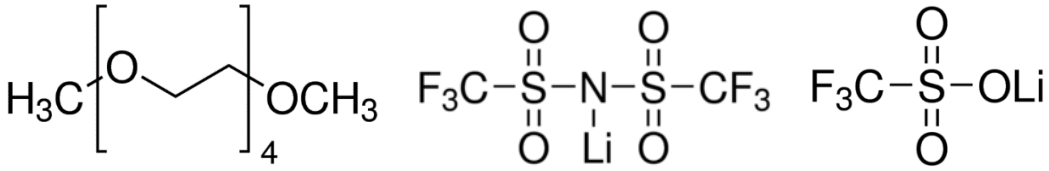

(a) (b) (c)

Figure 3.8 Chemical structure of (a) TEGDME, (b) LiTFSi and (c) Lithium triflate.

The purpose of using lithium salt is not only enhancing the conductivity of the Lithium-ion while redox happening but strengthening and fastening the formation of SEI (Solid-electrolyte interface) and as a result prevent the early-stage battery degradation [62]. Furthermore, a recent study provided by Luis A. et al [60] studied the possibility of the formation of the complex between a Li^+ (provided by Lithium salts, e.g. LiTFSi) and solvent molecule species as the concentration of Li salt becomes higher. This phenomenon called Solvated ionic liquids (SILs). This might help explain the improved conductivity of electrolytes, as the transference number of Lithium will increase. At the same time, the formation of the 3-D tunnel might not only helps limit the decomposition of tetraglyme but also favor the transformation of the Li^+ while charge/discharge. This research gives an idea that the concentrated electrolyte could be applicable to extend the battery life and definitely worth to develop in the future work.

The Li-salt chosen in this research involves both Lithium Salts listed in Figure 3.8 (b) and (c). Generally speaking, there are no major differences regarding morphology and cycling test result with two separate electrolytes that contains the listed two salts. Besides, the purpose that chosen to be as Li salt for Li-O_2 batteries is identical, that explains why the chemical structure of two Li salts is similar to each other. If not especially noted, the electrolyte using for this research is 1M LiTFSi in tetraglyme (TEGDME).

3.3 Effect of water in aprotic electrolyte

Other than selected components, some other impurity elements are also non-negligibly affecting the cell performance of Li-O_2 batteries. Water, the most undesirable components inevitably appear in aprotic electrolytes. Exploring the affection as well as the elimination of water in Li-O_2 cells will undoubtedly promote the efficiency and cyclability that will consequently extend the battery life.

Researchers have found that although the water in electrolytes could affect the morphologies of discharge products and enhance the capacity while discharge, its presence in electrolytes or O_2 atmosphere are in responsible of rapid charge voltage increase and hence cause cell death after limited cycles [63-66]. In addition, Li et al. [64] proposed that other than main discharge product Li_2O_2, a side product LiOH was also detected. More interestingly, they also announced that the presence of water is favorable to the transformation of the discharge product from Li_2O_2 to LiOH and its following decomposition on charging. Eventually, the charge over-potential could be effectively reduced. Apart from the mainstream thought, Li et al. [64] also demonstrated that the decomposition of LiOH is strongly dependent with the utilized catalysts, like Ru nanoparticles catalyst along with Super P electrode.

From information provided, a comparison of performance test was designed to justify whether the presence of water could have the same effect with nano-sized Ir particles. As shown in Fig 3.9, the Ir-rGO cathode is picked from the same fabrication batch. Both cathodes, as well as glass-fiber separator, were heated in a Vacuum oven at 110°C for 2h to eliminate the residue of water contents. The current density used was 0.013mA/cm^2 for both cells. The only variable parameter is the water content in the electrolyte. Fig 3.7 (a) uses the electrolyte that contains 88 ppm of water. Since both Li salt and electrolyte solvent are mixed as received from its commercial casting. Whereas the other cell was using the electrolyte with only 17ppm of water since both Li salt and tetraglyme solvent was dehydrated before mixing (Li salt was heated in a Vacuum oven for certain time, and tetraglyme was soaked with activated 3Å molecular sieves for a week).

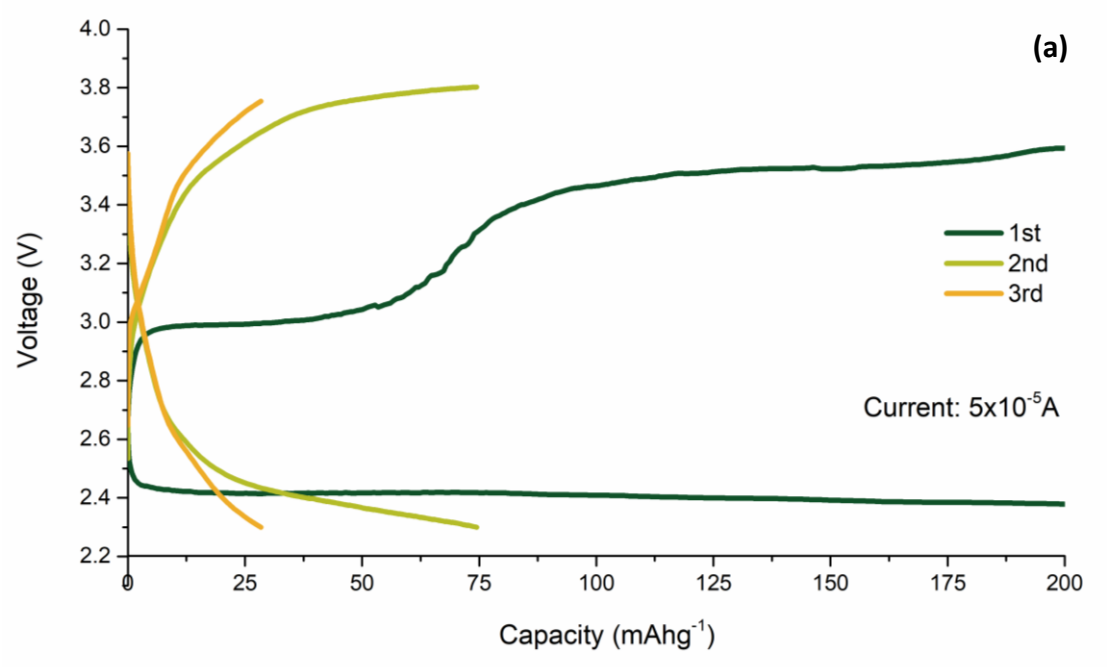

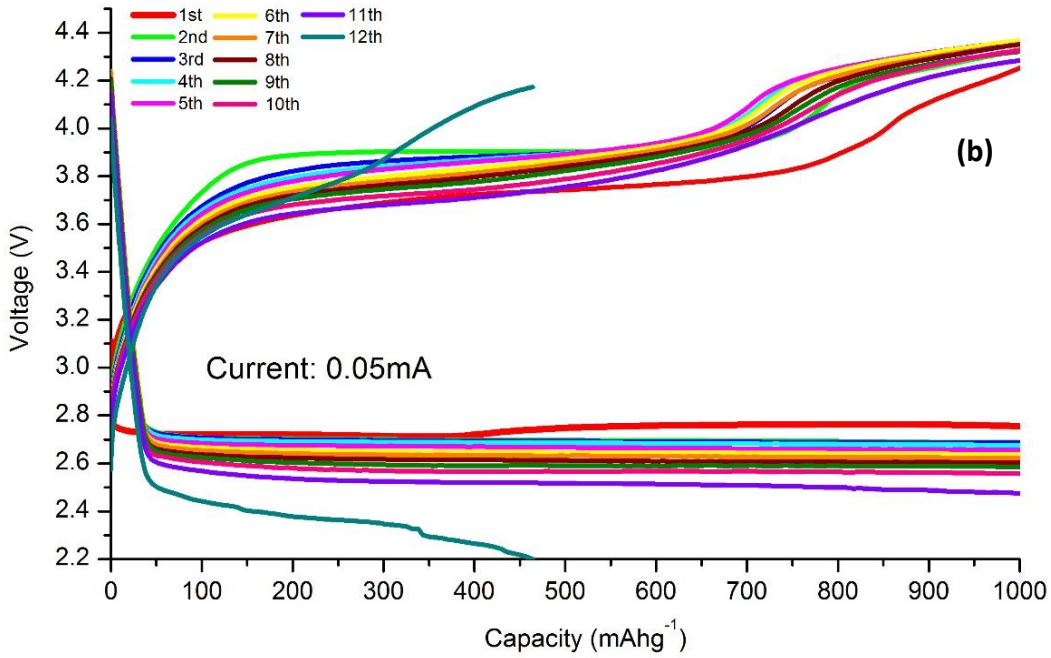

Figure 3.9 the Li-O_2 battery cycling test with Ir coated rGO cathode, the water content of both cells is (a) 88ppm, (b) 17ppm.

The redox efficiency for both cells appears to be promising at the initial stage, which indicates the functional effectiveness of Iridium nanoparticles as the catalyst. However, the results show drastic deviation regards to the cycle life. Even though the testing time for 3.9 (a) was only 20% from the testing time of 3.9 (b), the lower capacity did not help much as the battery only runs for 3 cycles along with the severe capacity loss. As a contrast, the second cell runs for more than 10 cycles without capacity loss and eventually failed at the 12^{th} cycle, not to say the capacity is 5 times larger than the formal cell. The only explanation is due to the dehydration process of the electrolyte, the side reaction with LiOH is prohibited due to the limited quantity of water in solution. This also helps to prevent the clogging and side product insulation on the surface of carbon cathode, as a result, the decomposition of both electrode and electrolytes could be efficiently protected.

Apparently, the conclusion from Li et al. [64] did not work the same with the Ir catalyzed rGO cathode for Li-O_2 battery. On the contrary, the result is identical with most of the commonly acknowledged concepts that water will be the major factor which eventually ruins the Li-O_2 battery that using aprotic electrolytes [63-66]. In fact, further investigation with water in aprotic electrolyte shows that with all the other parameters remain identical, the less the water is in the electrolyte, or in the whole aprotic Li-O_2 battery system, the longer lifetime it can achieve. As the data shown in Figure 4.7 (page 73), the water contents for the electrolyte before serving is only 0.4 ppm, and eventually, the battery runs for over 70 cycles with only moderate capacity loss, the total testing time for that is almost two months, which is a truly strengthening to the conclusion we proposed.

4. Results and Discussion of applied catalytic electrodes[3]

4.1 Pristine carbon electrode

The catalysis test result could only be persuasive if we make sure all the other parameters are fixed and perfected to its best condition. That is to say, for example, the selection of electrode substrate or the type and condition of the electrolyte that is going to utilize for the battery, must not be the main factor that simply leads the death of functional of the batteries. All the details regarding exploring the selection of the battery parts except catalyst are investigated deeply before the catalysis exploration and explained in Chapter 3.

With the confidence of other affective factors, the catalysis test starts with the baseline investigation. To be more exact, non-catalyzed carbon cathode has to be presented first as a comparison in order to justify the function and feasibility of the catalyzed samples. At the earlier stage of the investigation, another type of carbon called Super P is also tested to see the performance as used for carbon holder materials. However, the super P results showed in Figure 4.1 (a) only runs for 2 cycles with the energy efficiency of only 60%. The sample after cycling test was then immediately disassembled from the cell and the characterization by Raman and SEM was applicated and showed in Fig 4.1 (b) and (c), respectively. Raman result shows other than G and D band from carbon, there is no additional peak. This reveals that

[3] Part of the work was previously published as Wang, H-H., et al., (2017) Lithium Superoxide Hydrolysis and Relevance to Li-O_2 Batteries. The Journal of Physical Chemistry C. 121(18): p. 9657-9661.

neither the side product like LiOH or Li_2CO_3 was generated nor the intermediate discharge product, LiO_2 was stabilized and remained on top of the cathode. From Figure 4.1 (c), the major discharge product is concluded to be Li_2O_2 as the whole surface of the cathode was covered by the toroid-shaped “donut”, which was reported by several researchers already [21, 26, 49, 50, 60, 67]. However, the reason why Li_2O_2 could not be detected by Raman even though the existence of it was confirmed by SEM still remains unexplainable.

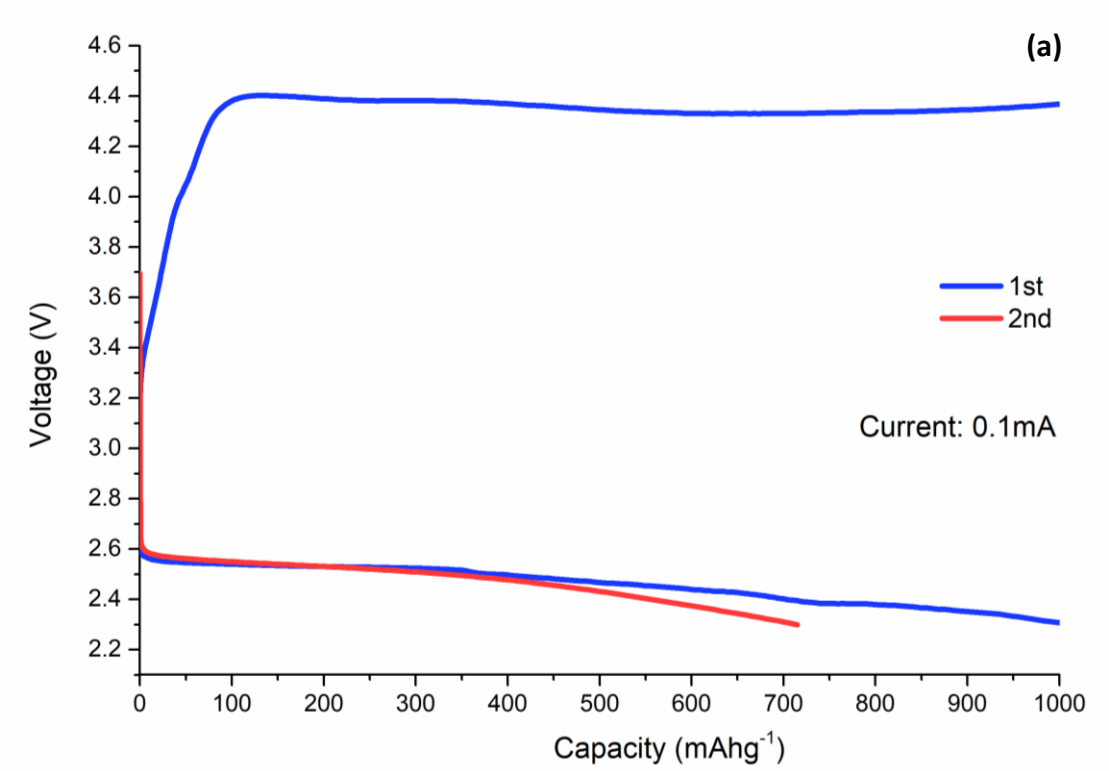

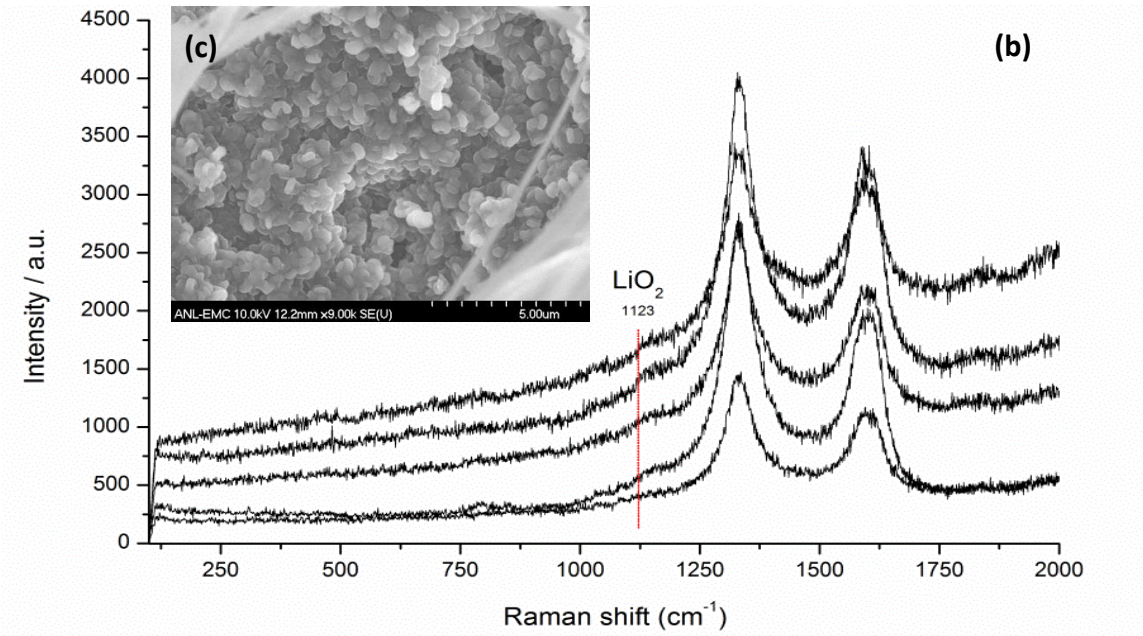

Figure 4.1 the (a) battery testing results, (b) Raman spectra and (c) SEM picture of cathode morphology after discharging with Iridium-coated super P carbon cathode.

With the same type of electrolyte, the pristine rGO can runs for 4 cycles with higher efficiency, approximately 70% while redox. The Raman data are shown in Figure 4.2 (b) indicates there was no side product generated either after the battery died since the only two major peaks are also from carbon. However, unlike the super P cathode that without any superoxide after discharging, the rGO cathode shows two weak peaks at both 1125 and 1500 cm^{-1}, which are believed as the existence of Lithium superoxide in terms of previous investigation [21, 42, 50, 67, 68]. The SEM images are shown in Figure 4.2 (c) verified the conclusion of existing superoxide, since there are no major toroids (only localized Li_2O_2 toroids observed, as marked by the red circle shown in Fig 2.4 c) shaped Li_2O_2 agglomeration observed with similar capacity, as the super P cathode is all covered with Lithium peroxide.

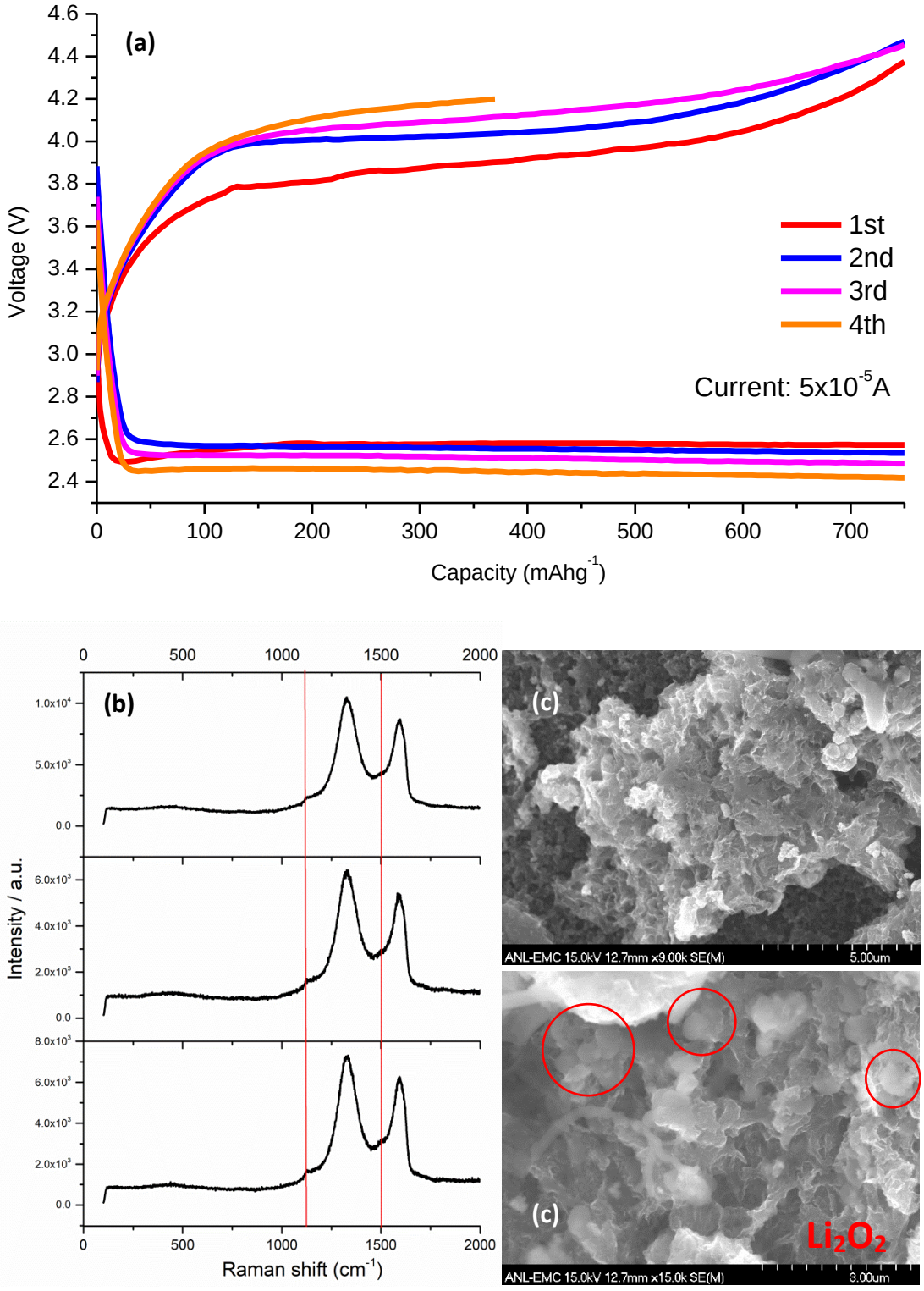

Figure 4.2 the (a) battery testing results, (b) Raman spectra and (c) SEM images of cathode morphology after discharging a non-catalyzed rGO electrode.

In conclusion, based on the comparison results presented from both Super P and rGO electrodes, rGO wins its spot as carbon holder utilized with the Li-O_2 battery in terms of its higher cyclability with same electrolyte, as well as higher LiO_2 to Li_2O_2 ratio. Based on the proposed mechanics of Li-O_2 battery (chapter 1.5.2, p12), the higher the ratio is, he lowers the energy barrier it needs to be reached during each cycle. In another word, a higher ratio of LiO_2 to Li_2O_2 could ensure the energy barrier from each cycle becomes easier to reach and as a result, lower the decomposition resistivity. In consequence, the cell efficiency, as well as cyclability, could be reasonably improved.

4.2 Iridium rGO as electrode

Talking about the noble metal as catalyst, Zhou W et al. [43] published a paper at 2015 indicated that a Li-O_2 battery with high rate cyclability and cycling stability can be reached by utilizing the iridium nano-crystal functionalized rGO cathode. At the same time, at 2016, Lu et al. [21] proposed that with the utilization of the similar iridium cathode in the Li-O_2 battery, the crystalized Ir_3Li was observed while the electrochemistry reaction proceeds with an Iridium rGO cathode. The Ir_3Li was characterized by HR-TEM and further justified with DFT calculation. The formation of Ir_3Li was explained by interstitial penetration of Li^+ into iridium particles. Furthermore, as presented in Fig 4.3, the DFT calculation of the lattice match between LiO_2 and Ir_3Li indicated that the Ir_3Li was believed to act as bedding for epitaxial growth for crystalline LiO_2 in terms of lattice matching.

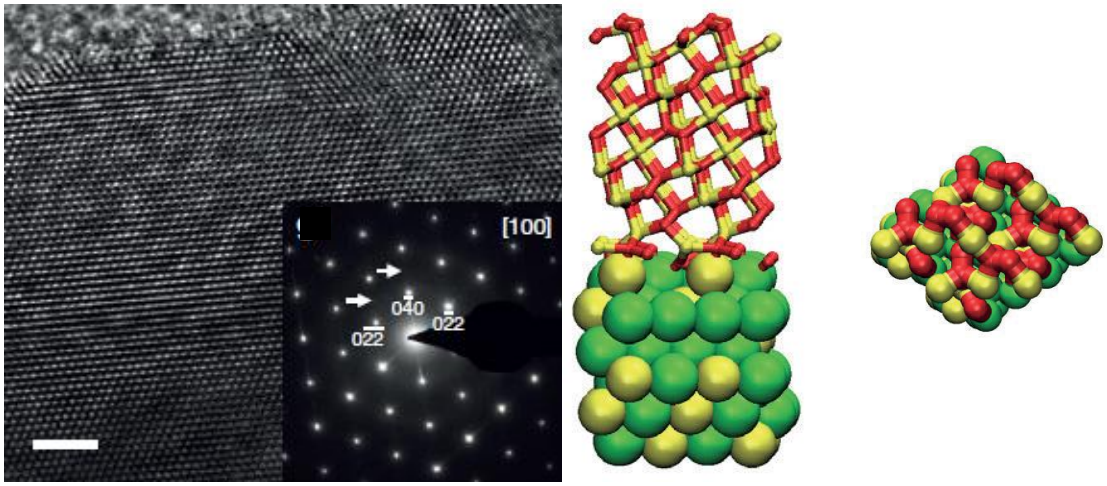

(a) (b)

Figure 4.3 (a) HR-TEM image of boxed area in e (scale bar, 2nm); and the corresponding electron diffraction pattern along the {1.0.0} zone axis giving evidence for the formation of an Ir_3Li intermetallic. The indices are diffraction vectors. The weak superstructure is observed as indicated by arrows. (b) Schematic showing lattice match between LiO_2 and Ir_3Li that may be responsible for the LiO_2 discharge product found on the Ir–rGO cathode. The two structures at left are the side- and top-views representing epitaxial growth of crystalline LiO_2 in (111) orientation on a (121) facet of Ir_3Li (Li is yellow, O is red and Ir is green). Reprint from ref [21].

In this research, as the information provided above, the Ir_3Li that transformed from Ir nanoparticles are believed to favor the formation of LiO_2, which could eventually help improve the efficiency while cycling and eventually prompt longer battery life. At the beginning, the research starting with duplicate the work done by Lu et al [21] to justify whether Ir nanoparticles can be used as a catalyst for Li-O_2 battery. The battery cycling test with Ir-rGO is shown in Fig 4.4 (a). Compared to the result from pristine rGO that can only run for 4 cycles, an Ir coated rGO cathode with dehydrated electrolyte runs for 30 cycles without any capacity loss (shown in Fig 4.4 b).

Besides that, the calculated efficiency for this cell (calculated with Fig 4.4 c) is

reaching the highest at 80% for the third cycle, which is getting closer to the regular efficiency of well-developed Li-ion batteries (80% to 90%) [69]. Although the cell efficiency dropped to 70% as the cycle number increases, it still remains at the same level to the best that pristine rGO did at its earlier cycling stage. On the other hand, the charging potential becomes higher as the cell keeps running, from 3.5 to 4.2, whereas the discharge potential remains basically unchanged at 2.78V till the battery died. This implies that while the cycle proceeds, the decomposition of either electrode or electrolyte exists, and as a result, the accumulative side-products insulated the electrode.

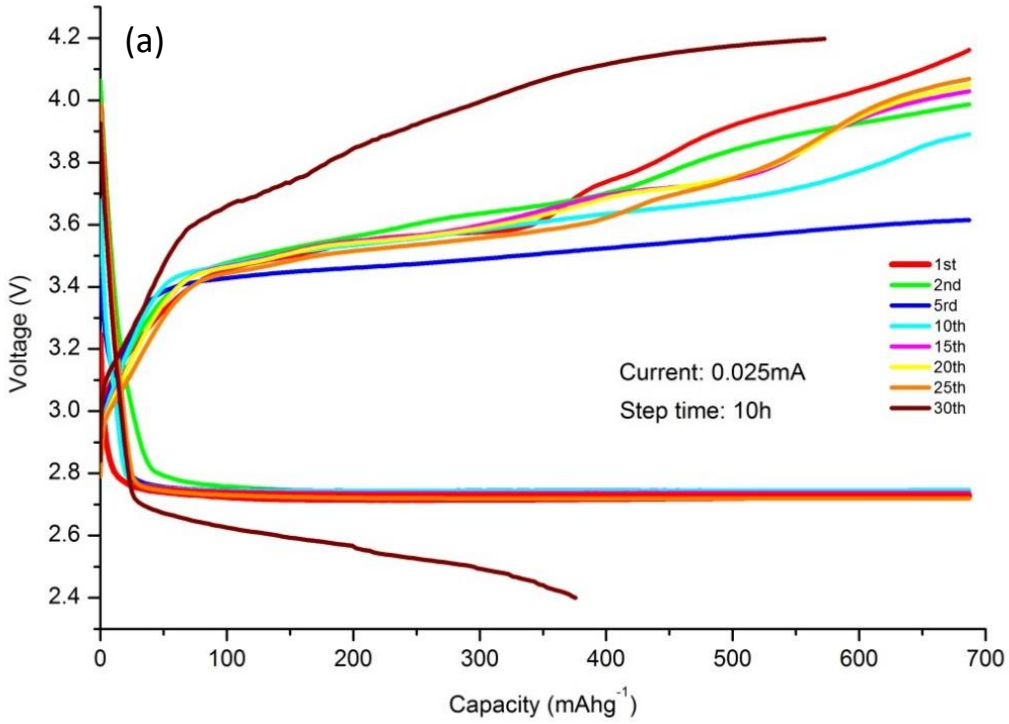

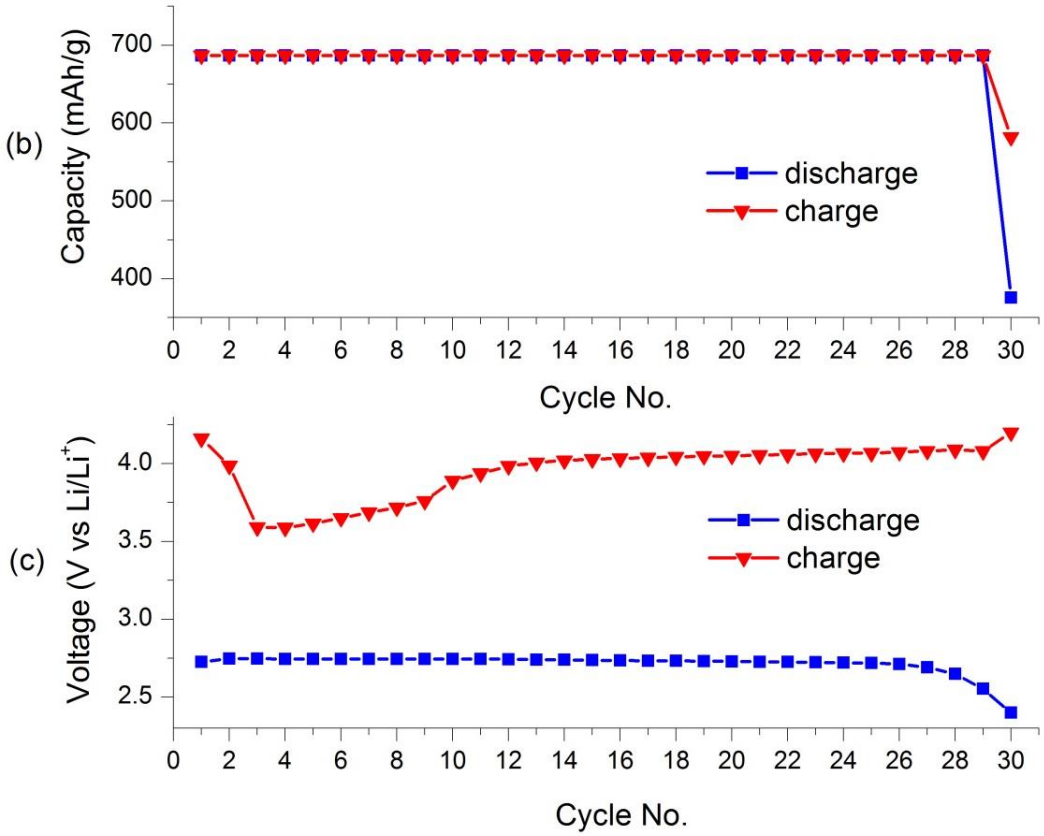

Figure 4.4 Performance of Li-O_2 battery with Ir-rGO cathode (a) battery cycling test, (b) the capacity of each cycle and (c) the voltages of the ending point of each discharge and charge step.

As shown in Fig 4.5 (a), compared to pristine rGO cathode, the two peaks located at 1125 cm^{-1} and 1500 cm^{-1} appears to be more noticeable, which implies the LiO_2 distribution becomes higher, or say the LiO_2 to Li_2O_2 ratio is higher than the pristine rGO cathode after discharge. Furthermore, the SEM images took from the sample after discharge shows very different morphology; apart from the morphology appears from non-catalyzed Super P and rGO electrode that the cathode was either partially or completely covered by "donut" Li_2O_2, there is no trace of the toroid-shaped Li_2O_2 as well as any other discharge products left. However, the peaks from Raman spectra indeed verified the existence of superoxide. Under this circumstance, Gittleson. F.S., et al., [68] gives an explanation said the discharge

product, LiO_2, accumulated in amorphous shape as the capacity increases instead of expecting crystal structured materials.

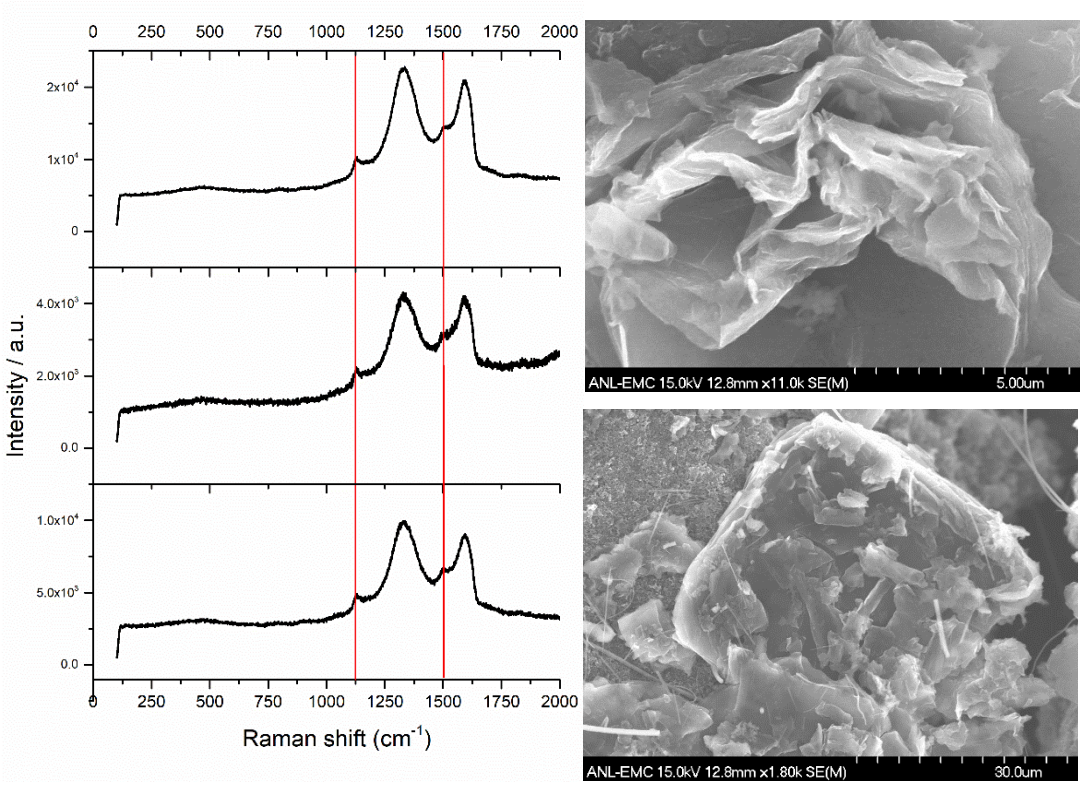

(a) (b)

Figure 4.5 (a) Raman spectra took from an Ir_3Li rGO cathode with a single discharge, and (b) SEM images of cathode show the morphology after discharging an Ir rGO cathode.

In conclusion, with the utilization of nano-sized Iridium as catalyst, the battery cyclability, as well as stability, has improved, besides that, the Raman and SEM results after characterization of cathode surface verified the results that the amorphous LiO_2 might become predominant as discharge product instead of Li_2O_2 that was normally observed in a non-catalyzed electrode cell.

4.3 $LiIr_3$ rGO as electrode

Then the idea came out as whether we can purposely support the Ir_3Li as catalyst on top of a carbon electrode in order to perfect the cycling performance. After the Ir_3Li was successfully synthesized (proposed in Chapter 2.2.1, P 26-28), the particles after grinding were blended with the slurry and further coated on top of cathode holder as the cathode for testing. The SEM images of the morphology of the surface of the electrode before testing are presenting in Fig 4.6 (a) and (b). As a comparison, Pristine rGO was also presented in Fig 4.6 (c) and (d). Based on SEM image took from Ir_3Li rGO cathode, we can observe there are clearly crystalline metal particles that stack on top of the rGO carbon holder, and the size of metallic particles differs from nano size to few micron and most of the single metal particle are stacked together with the size range of 1 to 10 μm.

An attempt to minimize the particle size was tested with the ionic shaker since a higher surface area is undoubtfully helpful to favor the crystalline LiO_2 stabilization and accumulation while discharging. However, Although the Ir_3Li are believed to be relatively inert in an air atmosphere, its hardness makes it difficult to grind with ball milling. Furthermore, because very few amount of samples (less than 5g in weight) were milled each time, so even the remained residue after milling is still considered over-wasted. As a result, the particle size minimization will be investigated in future work and the micron size Ir_3Li are applied as catalyst for all of the battery test and characterization.

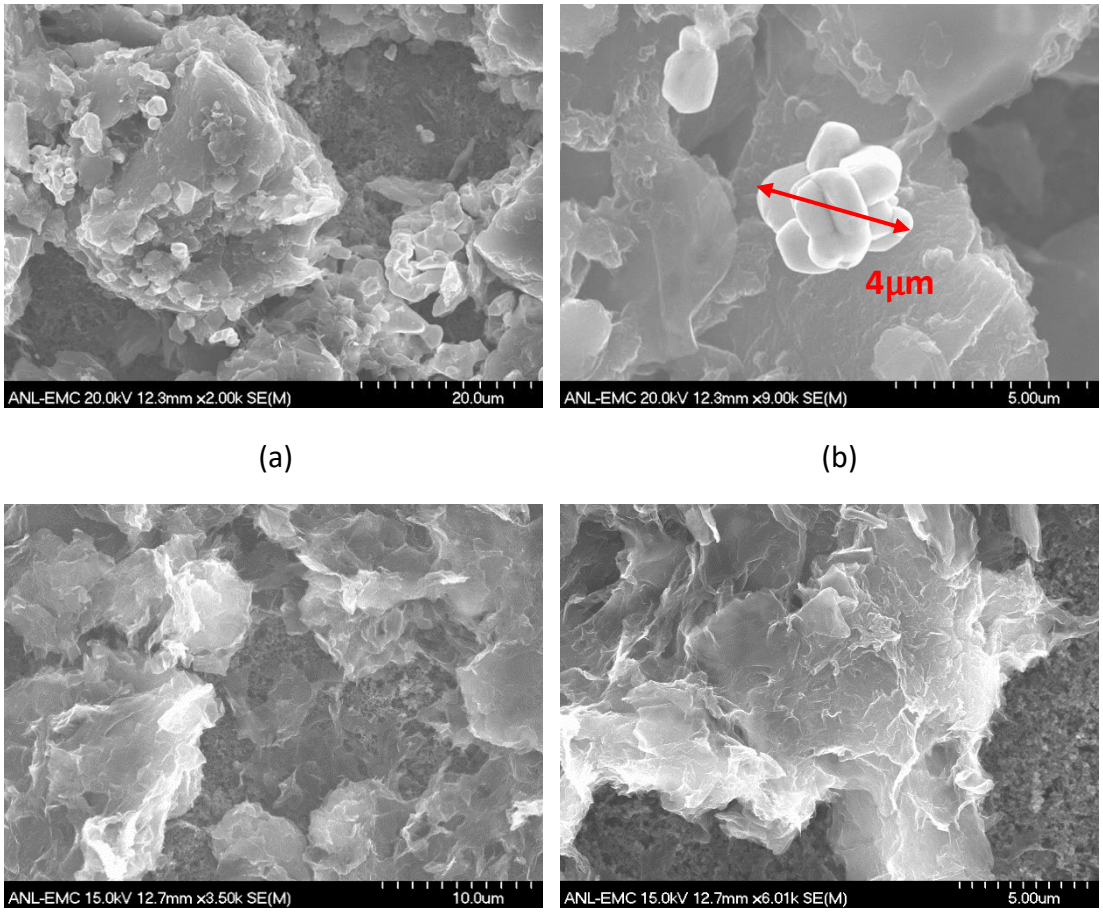

Figure 4.6 SEM image shows the morphology of pristine rGO cathode (a) and (b) with catalyst of $LiIr_3$ particles, (c) and (d) without any catalyst.

After the cathode was characterized, battery test was employed to test the cyclability in order to investigate the feasibility of catalytic performance of Ir_3Li metal in the Li-O_2 battery. As shown in Fig 4.7 (a), the battery cycling test result shows ultimate advanced cycling stability as well as repeatability. It runs for over 70 cycles with its original cell and gas atmosphere. Other than most of the improved cycling result with a Li-O_2 battery that reported by utilizing high current density, which leads a relatively short testing time (mostly reported for only 1 to 2 hours for each cycle). The purpose for this is to compress the cycling number before cathode decomposition or insulation [27, 33, 43]. On the other hand, the Ir_3Li catalyst can keep the cell durable

with a single testing time of 9 h. That is to say, the Li-O_2 cell with a metallic Ir_3Li catalyst could run continuously for more than 8 weeks without a severe capacity loss. It is an inevitable enhancement compared to all the other type of catalyzed Li-O_2 cells.

In the same Fig, we can also observe that a cut-off voltage has been set for charging potential at 4.2V; the purpose of setting this is to try to avoid exhausting or say over-pushing the battery to its full capacity while charging. With the common experience of Li-O_2 battery researchers, while the charging efficiency is lower than 70% or the charge potential is higher than 4.0V, the chance of cell decomposition, as well as cathode clogging or insulation, increases rapidly [2, 4, 8, 28, 60]. With the help of the cut-off charge voltage plus the functional catalyst, the factors that negatively affect the battery efficiency will be drastically minimized. As a result, the battery could run longer. Like shown in Fig 4.7 (b), after the charge potential was set to 4.2V, both charge and discharge potential show the solid result for the potential of each end testing point. This leads to an efficiency of 65%, which is lower than the ideal efficiency target.

Furthermore, the limitation of charge potential could also mean the capacity would have been blocked if the voltage reached the 4.2V limit before the charging step finishes. In Fig 4.7 (c), we can tell that it could always reach its full capacity with a low discharge overpotential, which means the mechanism involved while discharge is simple and smooth; whereas the charge capacity varies as test keeps running with the capacity loss from 0% to 12.5%. Here we excluded the 2^{nd} cycle since the initial stage of a running cell always possesses unexpected results; this stage was explained by the formation of the solid-electrolyte layer (SEI). At the 18^{th} cycle, the cell reaches its full capacity; other than that, the charge test was not complete due to the existence of cut-off voltage.

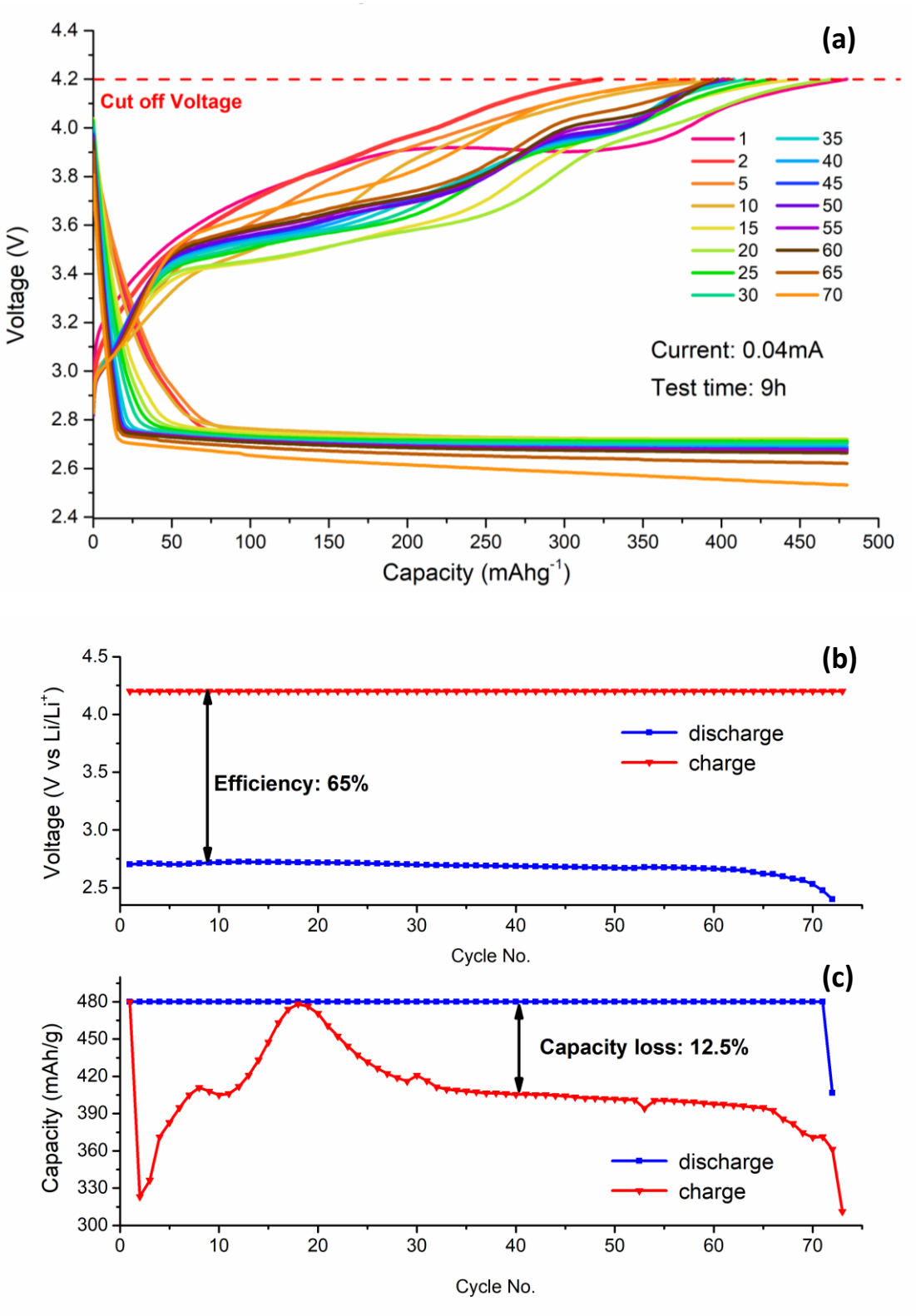

Figure 4.7 Performance of Li-O_2 battery with Ir_3Li-rGO cathode, (a) battery cycling test, (b) the voltages of the ending point of each discharge and charge step and (c) the capacity of the ending point of each discharge and charge step.

Compared to the cycling result from Ir rGO, we can make the conclusion that the high cyclability, as well as stability, has weak relation with low overpotential since we observe lower overpotential with Ir catalyzed cell instead of Ir_3Li as expected. However, the cycling performance did show better results with Ir_3Li compared to other cells. This implies that the mechanism proposed by Lu et al. was reliable; the battery could run with decreased energy barrier by the hypothesized mechanism. The difference in overpotential might cause by different size distribution between two catalysts. As mentioned earlier, the size of Ir_3Li varies from few hundred nanometers to a few microns, besides it always appears as aggregates, whereas the Ir particles were fabricated with “bottom-up” technique called chemical reduction. The size distribution of Ir has been characterized to be lower than a hundred nanometers. Since the size of two compared catalysts is not even on the same scale, this could explain why the higher overpotential happens with the Ir_3Li catalyzed cell. On the other hand, as mentioned, if the particle size could be effectively decreased, the cycling performance must be reasonably improved in terms of higher reactive surface area provided by nano Ir_3Li particles.

Furthermore, after 54 cycles, the battery efficiency starts to drop. However, after repurging the cell with high purity Oxygen, the cell recovered as efficiency increased to its normal stage. As a result, we believe this efficiency loss was caused by the imperfection of glass chamber sealing. This case eventually leads to low oxygen concentration around the cell and the efficiency decreases.

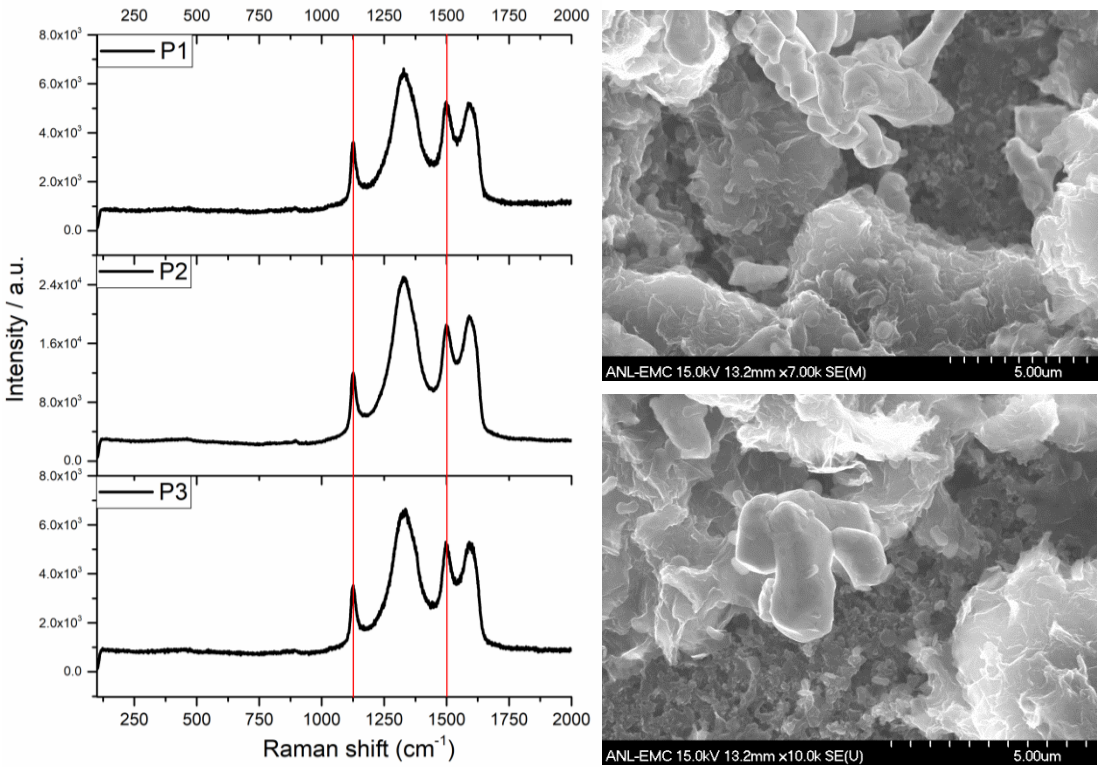

(a) (b)

Figure 4.8 (a) Raman spectra took from an Ir_3Li rGO cathode with a single discharge, and (b) SEM images of cathode show the morphology after discharging an Ir_3Li rGO cathode.

Similar to the results achieved from Ir rGO electrode, in Fig 4.8 (a), two Raman peaks located at 1125 cm^{-1} and 1500 cm^{-1} reveals the existence of LiO_2 with a single discharged $LiIr_3$ cell. The intensity of those two peaks from LiO_2 was even comparable to G-band carbon peaks that are much higher than the two observed with Ir rGO cell, this also reveals the LiO_2 to Li_2O_2 ratio is higher than the ratio in Ir coated cathode. From the SEM images provided in Fig 4.8 (b), the toroid-shaped Li_2O_2 was observed from the surface of the same $LiIr_3$ rGO cell after single discharging. However, with a high discharge capacity of 2400 $mAhg^{-1}$, the whole cathode should be covered with Li_2O_2 (see Fig 4.1 c), based on the theory that has been recognized by researchers, literally. However, only minor amount was witnessed after checking the whole

surface. Both of the results justified the feasibility of desirable battery mechanics, which has been shifted from a two-electron reaction (Li_2O_2) to a one-electron reaction (LiO_2).

To better understand the cathode morphology, one hypothesis is: instead of forming the crystallized structure, this cathode might cover by a large amount of amorphous LiO_2 since there is no critical evidence of any other discharge product had been formed with such that high capacity after discharging. Despite that, there is no evidence of any other critical discharge products or side products such as Li_2CO_3 and Li_2O_2 has been detected from the same electrode that characterized by Raman and SEM.

Eventually, after the Ir_3Li electrode was characterized by SEM and Raman, another characterization technique called titration was applied which can precisely determine the amount of peroxide existed on certain sample. With the titration result from peroxide, along with another simple calculation, the ideal Li_2O_2 to LiO_2 ratio could be figured out at last. In my previous work [70], although it was for exploring the hydrolysis of LiO_2, the detailed mechanism and procedure for this titration method were listed.

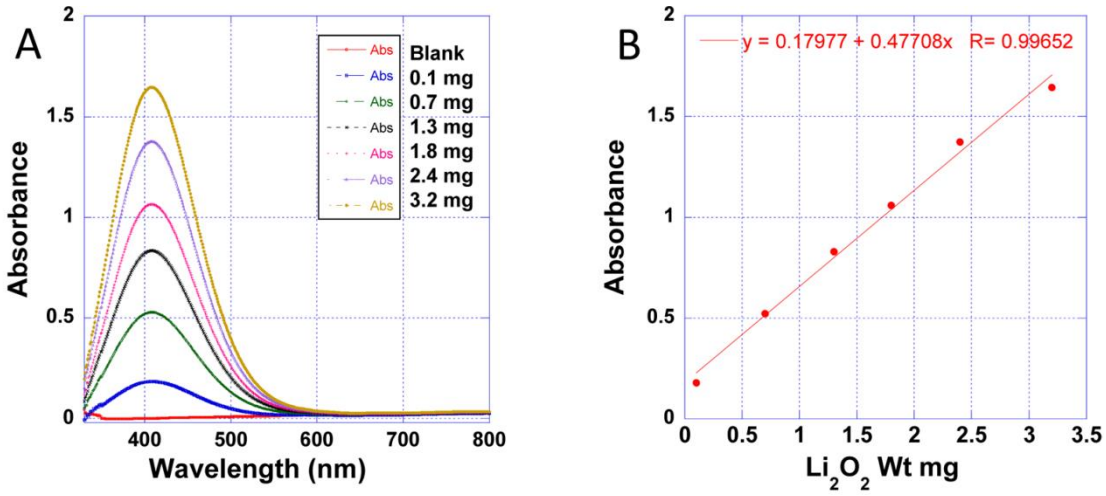

Figure 4.9 (A) UV−vis measurements (dual beam) of Li_2O_2 powders (Aldrich) added to 50 mL of TiOSO4 reagent (aq). (B) Calibration curve for Li_2O_2 in $TiOSO_4$. Reprint from ref [70].

Initially, a Li−O_2 cell with an Ir-rGO cathode identical to that used previously to produce a LiO_2 discharge product was run for one discharge cycle. The reaction of the LiO_2 discharge product with water was investigated using a spectrophotometric method to assess the amount of hydrogen peroxide produced. In this procedure, we first establish a calibration curve by adding incremental amounts of Li_2O_2 to the test reagent Ti(IV)OSO_4 (Aldrich, ~2 wt % in sulfuric acid), as shown in Figure 4.9 A and B. The discharge product LiO_2 on the Ir rGO cathode is then reacted with the acidic solution of Ti(IV)OSO_4 after the removal of the electrolyte but with the cathode material still present. Under the experimental conditions, Ti(IV) exists as TiO^{2+} (aq) complexed with SO_4^{2-} ion in 1.0 M H_2SO_4. This technique has been used previously for detecting formation of Li_2O_2, NaO_2, and KO_2 in M-O_2 electrochemical cells. It could be applied since the M-O_2 could react with water to form Li_2O_2 via equation (12) listed below:

$$M_2O_2 + 2H_2O \rightarrow 2MOH + H_2O_2 \qquad (12)$$

If hydrogen peroxide is present, then a color change to yellow/orange occurs due to the formation of a titanium peroxide complex, TiO_2SO_4. The acidity of the solution was found not to significantly affect the H_2O_2 detection [70].

With the technique listed above, half piece of Ir_3Li electrode after a single charge was dropped to the test reagent $Ti(IV)OSO_4$, the yellowish reagent after the reaction was then transferred to a 1cm path length cuvette for the UV-vis test. The result has shown in Fig 4.10 below. From the result, we can tell that although the total volume of titration indicator employed was only 5ml, the absorbance peak (0.119 in Abs) located at 406 nm was still lower than the standard usable zone for UV test, which has normally defined as 0.5 to 1.5 from Absorption. As a result, the total amount of Li_2O_2 formed while discharging is too low to be calculated. This also verifies the conclusion that the predominant discharge product for an Ir_3Li rGO electrode is LiO_2 instead of Li_2O_2 as expected.

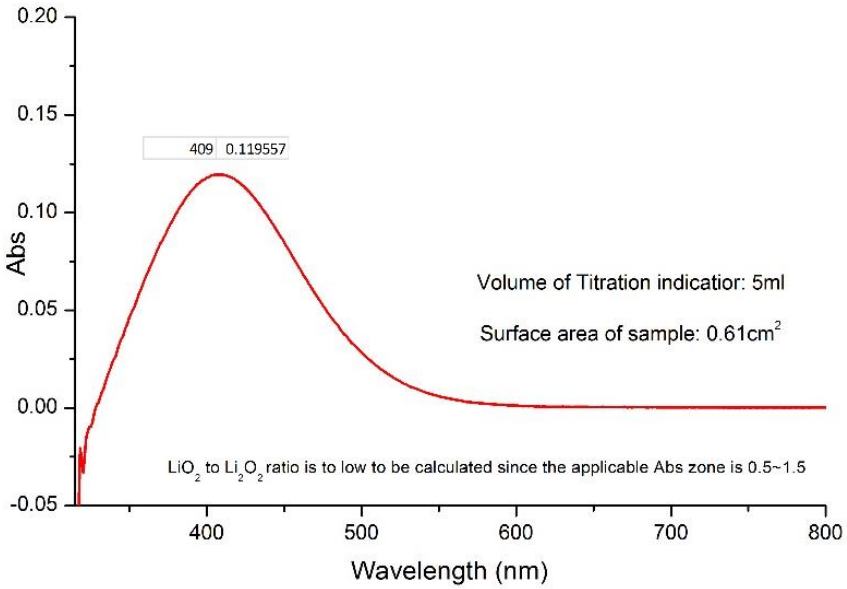

Figure 4.10 the UV-Vis result shows the absorbance peak of Titration indicator ($TiOSO_4$) for peroxides that provided from the same $LiIr_3$ rGO cathode.

4.4 Rh rGO as electrode

With all the information justified the noble metal iridium and its intermetallic Ir_3Li are literally feasible for utilizing as catalyst for the aprotic Li-O_2 battery system, one another idea came out as whether this catalytic effect could also exist with other noble metals, especially the one comes with the same group in the periodic table, Rhodium. The synthesize procedure was then developed, which uses the similar chemical reduction method with $RhCl_3$ and hydrazine hydrate.

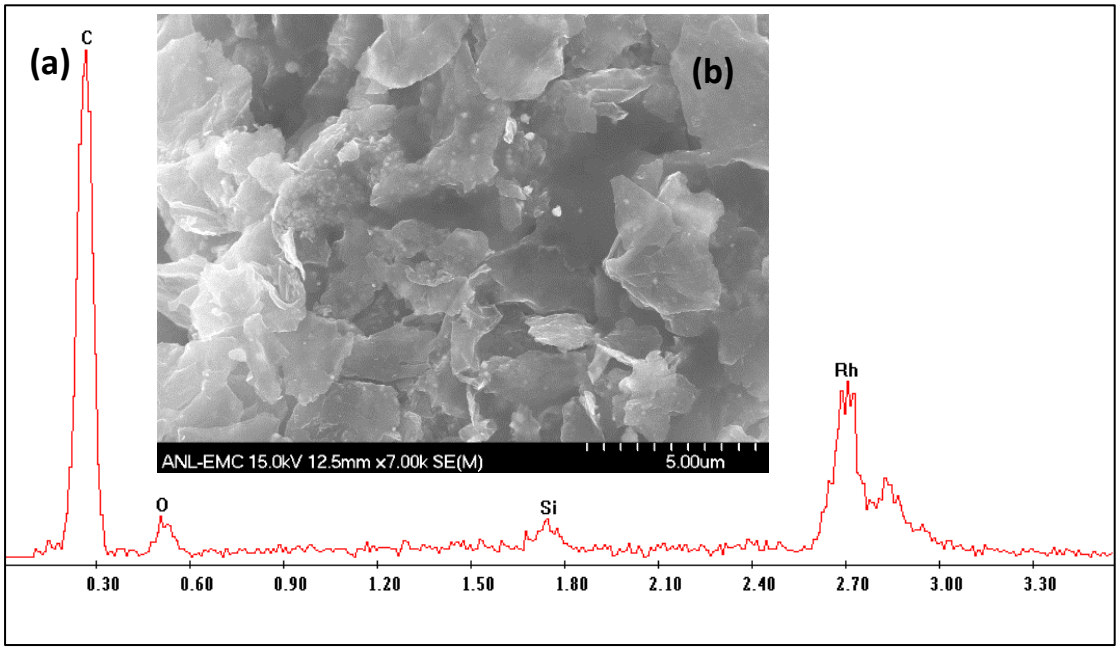

Figure 4.11 (a) EDAX spectra measured on top of the electrode surface with Rh rGO. (b) the SEM image took from a Rh rGO electrode before testing.

The existence of Rh nanoparticles is verified by EDAX that was shown in Fig 4.11 (a). Along with the SEM image in Fig 4.11 (b) which shows no indication of large-scale Rh particles, we can thus conclude that similar to the fabrication method of Ir rGO cathode, the nano-sized Rh rGO can be successfully synthesized by chemical reduction of $RhCl_3$. Other than that, the reduction from GO to rGO is further

confirmed which also verified the feasibility of this fabrication technique.

Again, the battery cycling result was also plotted and shown in Fig 4.12 (a) below. First, we can confidently state that nano-sized Rh particle is capable of being as one of another type of catalyst for Li-O_2 battery. Compare to both testing results from Ir and Ir_3Li catalyzed electrode, a Rh rGO cell performs similar cyclability as with Ir_3Li electrode for its cell efficiency as well as overpotential, yet the battery life is shorter, which only runs for less than 35 cycles. By contrast, an Ir_3Li cell runs for over 55 cycles whereas Iridium cell runs for only 30 cycles. Besides that, both Ir_3Li and Rh cell did not reach its full capacity due to the cut-off voltage setting. Surprisingly, this cut-off voltage setting, especially charge potential, did not affect the Ir rGO cell since all the charging potential from it was below the limitation line.

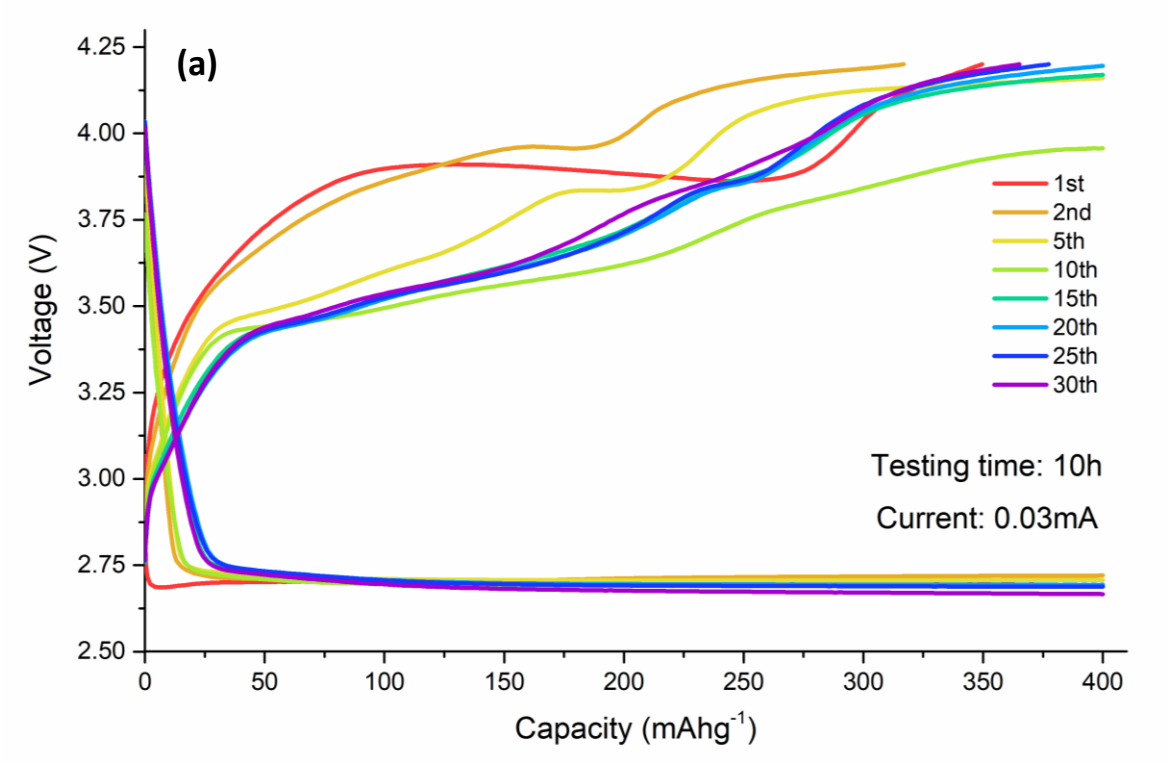

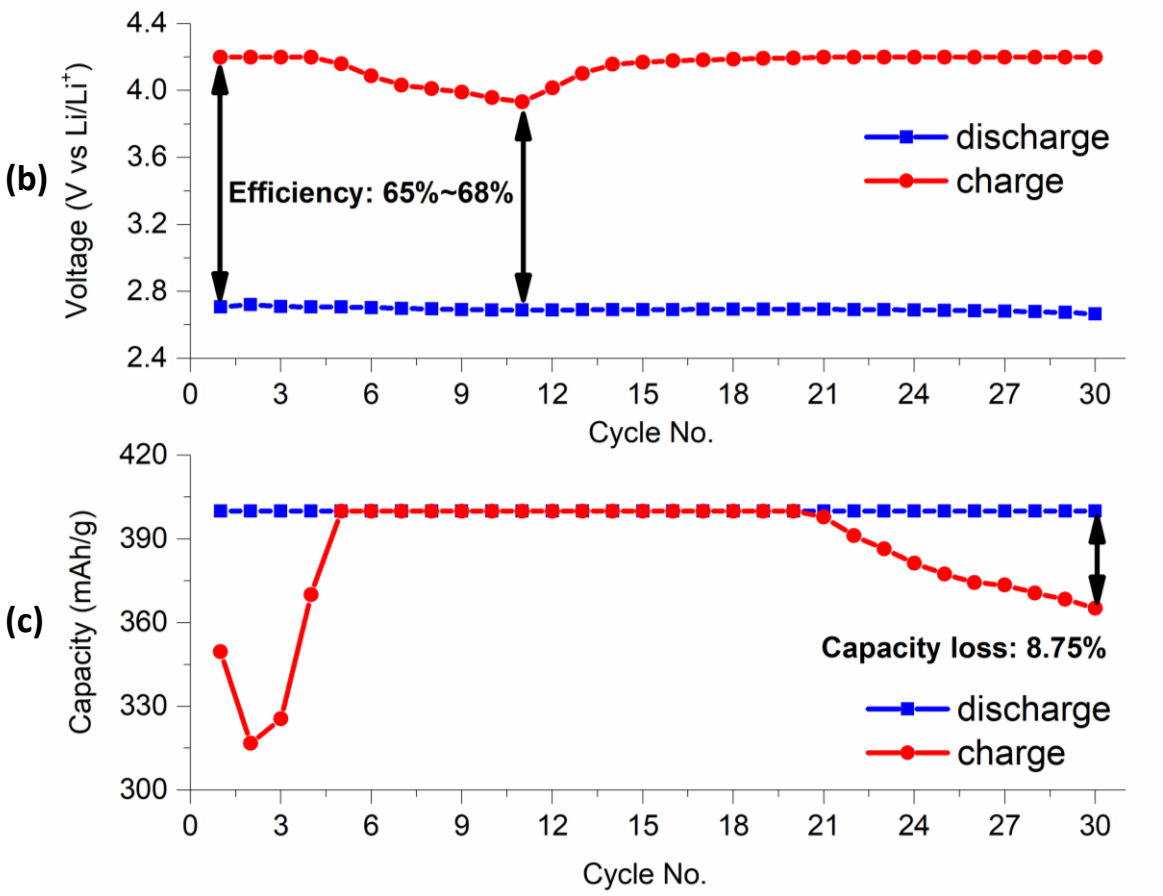

Figure 4.12 Performance of Li-O_2 battery with Rh-rGO cathode, (a) battery cycling test, (b) the voltages of the ending point of each discharge and charge step and (c) the capacity of the ending point of each discharge and charge step.

To be more exact, similar as the Ir_3Li cell, the battery efficiency was only 65% for most of the cycles after calculated with the results provided in Fig 4.12 (b), except a slight enhancement happened from the 5^{th} to 13^{th} with the efficiency increased from 65% to 68%. Even for that, the cell still processes lower efficiency than it was ideally targeted. In addition, the expected efficiency drop was also observed from the capacity data provided in Fig 4.12 (c). This abnormal circumstance that happened during the earlier stage of the test could be explained by the same hypothesis as stated for the formal cells that are due to the formation of the Solid-Electrolyte layer. The same evidence for all three catalyzed cells regard to this case is the efficiency

starts to recover at the end of this stage. Moreover, the cell even reaches its highest efficiency right after this stage, which reveals the formation of SEI was complete.

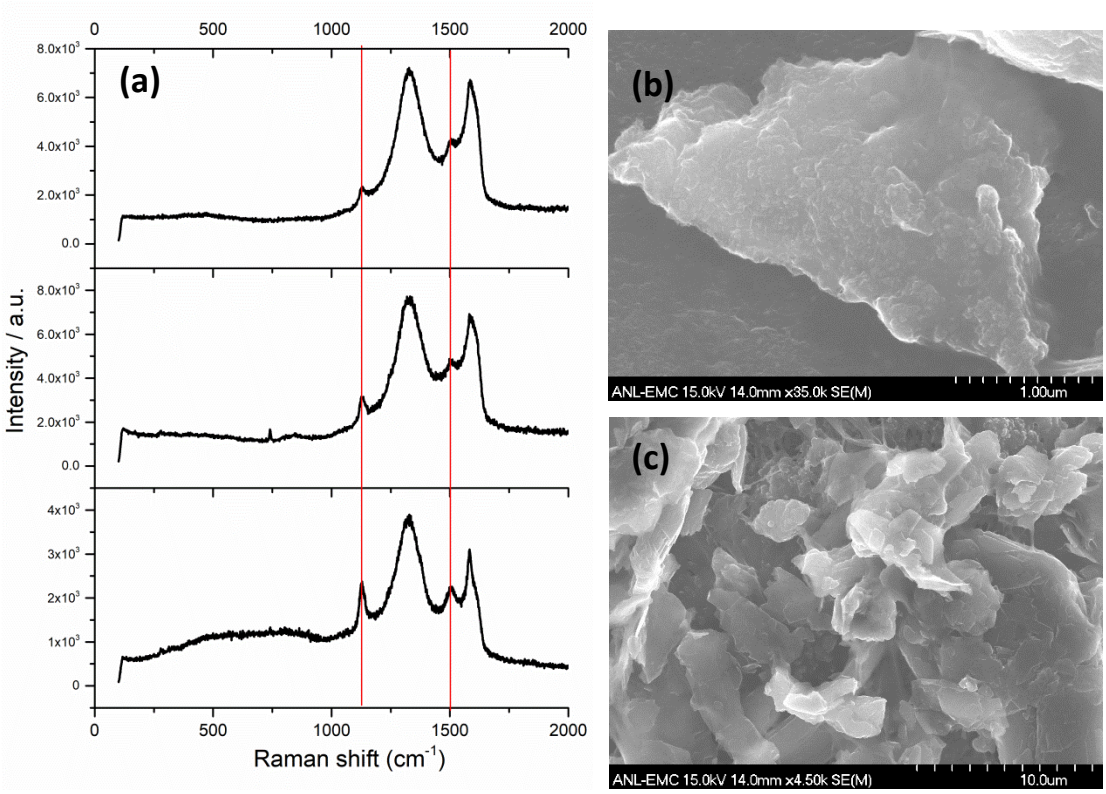

Figure 4.13 (a) Raman data of Rh rGO cathode after a single discharge, (b) and (c) SEM images of cathode morphology before discharging with Rh rGO cathode.

Same as the Iridium and Ir_3Li cells, Raman and SEM investigation was also applied to a single discharge Rh cell in order to explore the discharge products. From the Raman spectra presented in Fig 4.13 (a), LiO_2 peaks which located at 1125 cm^{-1} and 1500 cm^{-1} was always observed within random spots chosen from cathode surface; the intensity of those two peaks varies as we shift the testing spot. Besides that, there were no additional peaks appeared other than two from G- and D- band carbon baseline. Plus, from the SEM images provided in Fig 4.13 (b) and (c), the morphology picture took from a discharged cathode shows no characteristic discharge products

have formed, such as “donut” shaped Li_2O_2 or dendrite-shaped Li_2CO_3. In addition, same as the former 2 cells, the images indicate the electrode surface after discharge was identical to a un-tested pristine Rh cathode, basically; this means the LiO_2 could be formed as amorphous structure and dominated on top of the cathode.

In conclusion, other than those 2 un-catalyzed cells that have been characterized by the existence of crystallized Li_2O_2 as well as low LiO_2 to Li_2O_2 ratio, all the rest of three rGO electrodes that doped with Iridium, Iridium Lithium intermetallic and Rhodium appears with functional catalytic effects in terms of its cyclability, stability as well as relatively high efficiency. Furthermore, those three catalyzed electrodes show identical results after characterized by SEM and Raman, which indicates that the predominant discharge product is Lithium superoxide instead of Lithium peroxide. Moreover, it was most likely formed and stabilized with an amorphous non-crystalized shape followed with an epitaxy mechanism, which requires the introduction of noble metal to be provided as a function of growth bedding.

5. Conclusions

In order to ascend the battery performance of the Li-O_2 battery, multiple attempts were employed via a variety of aspects including selection of components, perfection of fabrication technique and introduction of new catalytic materials. At the end, the cell that possessed with all those fixed applications was tested and characterized. The results indicate that:

1. Compared to a un-catalyzed carbon electrode, a noble metal-doped (Iridium, Rhodium and Lithium-Iridium intermetallic alloy) electrode always runs with higher cyclability, stability as well as resistivity. To be more exact, with the same type of electrolyte, the metallic catalyzed cell always runs up to 50 to 60 cycles with a reliable testing cycle time, whereas the pristine could only run for less than 5 cycles.

2. The theoretical mechanism was also described for this improvement as the initiation of an epitaxial growth from an overlayer of LiO_2 onto the crystalline layer of noble metal. The discharge product for each catalyst was characterized by Raman and SEM techniques, etc.

3. A new titration method imported from the previous work was also applied to better evaluate the LiO_2 to the Li_2O_2 ratio as designed. These results revealed that in favor of epitaxy effect, the meta-stable discharge intermediate, LiO_2, could be efficiently stabilized. Eventually, it will become the predominant discharge product instead of widely acknowledged Li_2O_2. As a result, the energy barrier that needs to be overcome while redox will be significantly reduced.
4. Despite from catalyst, a variety of fabrication technique was investigated to

develop a better cathode material as well as electrode bedding. After incalculable implementation, it has been settled to utilize a GDL carbon holder coated with PVDF blended slurry that contains with chemically reduced Graphene Oxide (rGO) carbon, because it shows the best conductivity as well as gas permeability that an electrode would need.

5. Another effective factor, like the condition of electrolyte, was also studied in this research; water becomes the most undesirable component in the aprotic Li-O_2 battery since it is significantly favorable to the formation of side products, such as LiOH or Li_2CO_3, and eventually responsible for the rapid death of any kind of aprotic cell.

References

1. Padbury, R. and X. Zhang, *Lithium-oxygen batteries—Limiting factors that affect performance.* Journal of Power Sources, 2011. **196**(10): p. 4436-4444.
2. Girishkumar, G., et al., *Lithium-Air Battery: Promise and Challenges.* J Phys Chem Lett, 2010. **1**(14): p. 2193-2203.
3. Richter, B., et al., *Energy Future: Think Efficiency.* 2008, American Physical Society: College Park, MD.
4. Lu, J., et al., *Aprotic and aqueous Li-O_2 batteries.* Chem Rev, 2014. **114**(11): p. 5611-40.
5. Shao, Y., et al., *Making Li-Air Batteries Rechargeable: Material Challenges.* Advanced Functional Materials, 2013. **23**(8): p. 987-1004.
6. Feng, N., P. He, and H. Zhou, *Critical Challenges in Rechargeable Aprotic Li-O2Batteries.* Advanced Energy Materials, 2016. **6**(9): p. 1502303.
7. Kraytsberg, A., and Y. Ein-Eli, *Review on Li-air batteries—Opportunities, limitations and perspective.* Journal of Power Sources, 2011. **196**(3): p. 886-893.
8. Imanishi, N., P. Bruce, and A.C. Luntz, *The lithium air battery: fundamentals*. 2014, New York: Springer.
9. Transportation.gov. *Corporate Average Fuel Economy (CAFE) Standards*. 2014.
10. *Solid State Batteries*, in *Energy Storage Association*. 2017.
11. Gao, J., *Design, Improvement and Fundamental Studies on Arpotic Lithium-Oxygen Batteries*, in *Civil and Materials Engineering* 2015, University of Illinois at Chicago. p. 120.
12. Yan, H., et al., *Electrochemical reduction approach-based 3D graphene/Ni(OH) 2 electrode for high-performance supercapacitors.* Electrochimica Acta, 2015. **154**: p. 9-16.
13. *The Lithium-Air battery: fundamentals*, ed. P. Bruce. Springer: Springer.
14. Jung, H.G., et al., *An improved high-performance lithium-air battery.* Nat Chem, 2012. **4**(7): p. 579-85.
15. McCloskey, B.D., et al., *Mechanistic insights for the development of Li-O_2 battery materials: addressing Li_2O_2 conductivity limitations and electrolyte and cathode instabilities.* Chem Commun (Camb), 2015. **51**(64): p. 12701-15.
16. Littauer, E.L., and K.C. Tsai, *Anodic Behavior of Lithium in Aqueous Electrolytes.* J. Electrochem. Soc., 1976. **123**(6): p. 771-776.
17. Abraham, K.M., and Z. Jiang, *A Polymer Electrolyte-Based Rechargeable Lithium/Oxygen Battery.* J. Electrochem. Soc., 1996. **143**(1): p. 1-5.
18. *LI-s and LI-O2 batteries with high specific energy*. 2016, New York, NY: Springer Berlin Heidelberg. pages cm.

19. McCloskey, B.D., et al., *Solvents' Critical Role in Nonaqueous Lithium-Oxygen Battery Electrochemistry.* J Phys Chem Lett, 2011. **2**(10): p. 1161-6.
20. Hummelshoj, J.S., et al., *Communications: Elementary oxygen electrode reactions in the aprotic Li-air battery.* J Chem Phys, 2010. **132**(7): p. 071101.
21. Lu, J., et al., *A lithium-oxygen battery based on lithium superoxide.* Nature, 2016. **529**(7586): p. 377-82.
22. Xie, J., et al., *Achieving Low Overpotential Li-O_2 Battery Operations by Li_2O_2 Decomposition through One-Electron Processes.* Nano Lett, 2015. **15**(12): p. 8371-6.
23. Liu, T., et al., *Cycling Li-O_2 batteries via LiOH formation and decomposition.* Science, 2015. **350**(6260): p. 530-533.
24. Stankovich, S., et al., *Graphene-based composite materials.* Nature, 2006. **442**(7100): p. 282-6.
25. Burke, C.M., et al., *Enhancing electrochemical intermediate solvation through electrolyte anion selection to increase nonaqueous Li-O_2 battery capacity.* Proc Natl Acad Sci U S A, 2015. **112**(30): p. 9293-8.
26. Lu, J., et al., *A nanostructured cathode architecture for low charge overpotential in lithium-oxygen batteries.* Nat Commun, 2013. **4**: p. 2383.
27. Ottakam Thotiyl, M.M., et al., *A stable cathode for the aprotic Li-O2 battery.* Nat Mater, 2013. **12**(11): p. 1050-6.
28. Luntz, A.C. and B.D. McCloskey, *Nonaqueous Li-air batteries: a status report.* Chem Rev, 2014. **114**(23): p. 11721-50.
29. Ogasawara, T., et al., *Rechargeable Li2O2 Electrode for Lithium Batteries.* J Am Chem Soc, 2006. **128**(4): p. 1390-1393.
30. Ren, X., et al., *Understanding side reactions in K-O_2 batteries for improved cycle life.* ACS Appl Mater Interfaces, 2014. **6**(21): p. 19299-307.
31. Lei, Y., et al., *Synthesis of porous carbon supported palladium nanoparticle catalysts by atomic layer deposition: application for rechargeable lithium-O_2 battery.* Nano Lett, 2013. **13**(9): p. 4182-9.
32. Lu, Y.-C., et al., *The Influence of Catalysts on Discharge and Charge Voltages of Rechargeable Li–Oxygen Batteries.* Electrochem. Solid-State Lett, 2010. **13**(6): p. A69-A72.
33. Chen, Y., et al., *Charging a Li-O_2 battery using a redox mediator.* Nat Chem, 2013. **5**(6): p. 489-94.
34. WahLow., F., C. WeiLai, and S.B. Hamid, *Easy preparation of ultrathin reduced graphene oxide sheets at a high stirring speed.* Ceramics International, 2015. **41**(4): p. 5798-5806.
35. Marcano, D.C., et al., *Improved Synthesis of Graphene Oxide.* ACS Nano, 2010. **4**: p. 9.
36. Yu, H., et al., *High-efficient Synthesis of Graphene Oxide-Based on Improved Hummers Method.* Sci Rep, 2016. **6**: p. 36143.

37. Storm, M.M., et al., *Reduced graphene oxide for Li-air batteries: The effect of oxidation time and reduction conditions for graphene oxide.* Carbon, 2015. **85**: p. 233-244.
38. Stankovich, S., et al., *Synthesis of graphene-based nanosheets via chemical reduction of exfoliated graphite oxide.* Carbon, 2007. **45**(7): p. 1558-1565.
39. Lv, W., et al., *Low-Temperature Exfoliated Graphenes: Vacuum-Promoted Exfoliation and Electrochemical Energy Storage.* ACS Nano, 2009. **3**(11): p. 3730–3736.
40. H.C.Donkersloot and J.H.N.V. Vucht, *The crystal structure of IrLi, Ir_3Li and $LiRh_3$.* Journal of the Less-Common Metals, 1976. **50**(2): p. 279-282.
41. McCloskey, B.D., et al., *On the efficacy of electrocatalysis in nonaqueous Li-O_2 batteries.* J Am Chem Soc, 2011. **133**(45): p. 18038-41.
42. Gallant, B.M., et al., *Influence of Li_2O_2 morphology on oxygen reduction and evolution kinetics in Li–O_2 batteries.* Energy & Environmental Science, 2013. **6**(8): p. 2518.
43. Zhou, W., et al., *Iridium incorporated into deoxygenated hierarchical graphene as a high-performance cathode for rechargeable Li–O_2 batteries.* J. Mater. Chem. A, 2015. **3**(28): p. 14556-14561.
44. Vucht, J.H.N.V. and K.H.J. Buschow, *Note on the occurrence of intermetallic compounds in the Lithium-Palladium System.* J. the Less Common Metals, 1976: p. 345-347.
45. Sangster, J. and A.D.Pelson, *The Ir-Li (Iridium-Lithium) system.* J.Phase Equilibria, 1992. **13**(1): p. 59-62.
46. Tan, M., et al., *Active and regioselective rhodium catalyst supported on reduced graphene oxide for 1-hexene hydroformylation.* Catal. Sci. Technol., 2016. **6**(4): p. 1162-1172.
47. Shui, J.-L., H.-H. Wang, and D.-J. Liu, *Degradation and revival of Li–O_2 battery cathode.* Electrochemistry Communications, 2013. **34**: p. 45-47.
48. Peng, Z., et al., *A Reversible and Higher-Rate Li-O2 Battery.* Science, 2012. **337**(6094): p. 563-566.
49. Lu, J., et al., *Effect of the size-selective silver clusters on lithium peroxide morphology in lithium-oxygen batteries.* Nat Commun, 2014. **5**: p. 4895.
50. Zhai, D., et al., *Disproportionation in Li-O2 batteries based on a large surface area carbon cathode.* J Am Chem Soc, 2013. **135**(41): p. 15364-72.
51. Ding, Y. and Z. Zhang, *Nanoporous metals for advanced energy technologies*. 2016, Switzerland: Springer.
52. Pei, S. and H.-M. Cheng, *The reduction of graphene oxide.* Carbon, 2012. **50**(9): p. 3210-3228.
53. Ottakam Thotiyl, M.M., et al., *The carbon electrode in nonaqueous Li-O_2 cells.* J Am Chem Soc, 2013. **135**(1): p. 494-500.
54. Kim, J.G., et al., *$MnCo_2O_4$ nanowires anchored on reduced graphene oxide*

sheets as effective bifunctional catalysts for Li-O_2 battery cathodes. ChemSusChem, 2015. **8**(10): p. 1752-60.

55. Shukla, G. *Graphite Oxide, Graphene Oxide and the Reduced one*. 2015 December 3, 2015].
56. Wang, Z.-L., et al., *Graphene Oxide Gel-Derived, Free-Standing, Hierarchically Porous Carbon for High-Capacity and High-Rate Rechargeable Li-O_2 Batteries.* Advanced Functional Materials, 2012. **22**(17): p. 3699-3705.
57. Sevim, M., et al., *Bimetallic MPt (M: Co, Cu, Ni) alloy nanoparticles assembled on reduced graphene oxide as high performance cathode catalysts for rechargeable lithium-oxygen batteries.* Journal of Alloys and Compounds, 2016. **683**: p. 231-240.
58. Shin, H.-J., et al., *Efficient Reduction of Graphite Oxide by Sodium Borohydride and Its Effect on Electrical Conductance.* Advanced Functional Materials, 2009. **19**(12): p. 1987-1992.
59. Scheers, J., et al., *Life of superoxide in aprotic Li-O_2 battery electrolytes: simulated solvent and counter-ion effects.* Phys Chem Chem Phys, 2016. **18**(15): p. 9961-8.
60. Aetukuri, N.B., et al., *Solvating additives drive solution-mediated electrochemistry and enhance toroid growth in non-aqueous Li-O_2 batteries.* Nat Chem, 2015. **7**(1): p. 50-6.
61. Gittleson, F.S., et al., *Pt and Pd catalyzed oxidation of Li_2O_2 and DMSO during Li-O_2 battery charging.* Chem Commun (Camb), 2016. **52**(39): p. 6605-8.
62. Aravindan, V., Gnanaraj, J., Madhavi, S. & Liu, H. K. , *Lithium-ion conducting electrolyte salts for lithium batteries.* . Chem. Eur. J., 2011. **17**: p. 14326–14346.
63. Meini, S., Piana, M., Tsiouvaras, N., Garsuch, A. & Gasteiger, H. A. , *The effect of water on the discharge capacity of a non-catalysed carbon cathode for Li-O2 batteries.* Electrochem. Solid State Lett., 2012. **15**: p. A45-A48.
64. Li, F., et al., *The water catalysis at oxygen cathodes of lithium-oxygen cells.* Nat Commun, 2015. **6**: p. 7843.
65. Schwenke, K.U., Metzger, M., Restle, T., Piana, M. & Gasteiger, H. A., *The influence of water and protons on Li_2O_2 crystal growth in aprotic Li-O_2 cells.* J. Electrochem. Soc. , 2015. **162**: p. A573–A585.
66. Cho, M.H.e.a., *The effects of moisture contamination in the Li-O_2 battery.* Journal of Power Sources, 2014. **268**: p. 565-574.
67. Zhai, D., et al., *Raman Evidence for Late-Stage Disproportionation in a Li-O_2 Battery.* J Phys Chem Lett, 2014. **5**(15): p. 2705-10.
68. Gittleson, F.S., et al., *Raman Spectroscopy in Lithium-Oxygen Battery Systems.* ChemElectroChem, 2015. **2**(10): p. 1446-1457.
69. Arora, P. and Z. Zhang, *Battery Separators.* chem rev, 2004. **104**(10): p. 4419–4462.

70. Wang, H-H., et al., *Lithium Superoxide Hydrolysis and Relevance to Li-O_2 Batteries.* The Journal of Physical Chemistry C, 2017. **121**(18): p. 9657-9661.

Appendix

ACS Copyright Information

Parts of the results represented in Chapter 4, section 4.3 were published as manuscript for I was the fourth author. Reprinted with permission from Wang, H-H., et al., *Lithium Superoxide Hydrolysis and Relevance to Li-O_2 Batteries.* The Journal of Physical Chemistry C, 2017. **121**(18): p. 9657-9661. Copyright © (2017) American Chemical Society.

The copyright policies in this appendix are attached below from the website of the American Chemical Society (ACS) (https://s100.copyright.com/AppDispatchServlet).

RightsLink®

Home | Create Account | Help

Title: Lithium Superoxide Hydrolysis and Relevance to Li–O2 Batteries

Author: Hsien-Hau Wang, Yun Jung Lee, Rajeev S. Assary, et al

Publication: The Journal of Physical Chemistry C

Publisher: American Chemical Society

Date: May 1, 2017

LOGIN

If you're a copyright.com user, you can login to RightsLink using your copyright.com credentials. Already a RightsLink user or want to learn more?

PERMISSION/LICENSE IS GRANTED FOR YOUR ORDER AT NO CHARGE

This type of permission/license, instead of the standard Terms & Conditions, is sent to you because no fee is being charged for your order. Please note the following:

- Permission is granted for your request in both print and electronic formats, and translations.
- If figures and/or tables were requested, they may be adapted or used in part.
- Please print this page for your records and send a copy of it to your publisher/graduate school.
- Appropriate credit for the requested material should be given as follows: "Reprinted (adapted) with permission from (COMPLETE REFERENCE CITATION). Copyright (YEAR) American Chemical Society." Insert appropriate information in place of the capitalized words.
- One-time permission is granted only for the use specified in your request. No additional uses are granted (such as derivative works or other editions). For any other uses, please submit a new request.

If credit is given to another source for the material you requested, permission must be obtained from that source.

BACK | CLOSE WINDOW

Vita

NAME: Chengji Zhang

EDUCATION: B.Eng., Ceramic Engineering, Shenyang Ligong University, Shenyang, Liaoning, China, 2014

M.S., Materials Engineering, University of Illinois at Chicago, Chicago, Illinois, 2017

TEACHING: Teaching assistant of CME 260 - Properties of Materials, Spring 2016

Teaching assistant of CME 261 - Materials for Manufacturing, Fall 2016

PROFESIONAL EXPERIENCE: Guest Graduate Student, Materials Science Division, Argonne National Laboratory, Lemont, IL, 08/2015 - 10/2017.

PUBLICATION: Hsien-Hau Wang, Yun Jung Lee, Rajeev S. Assary and Chengji Zhang et al. *Lithium Superoxide Hydrolysis and Relevance to Li-O_2 Batteries,* Journal of Physical Chemistry C, 2017. **121**(18): p. 9657-9661. *DOI: 10.1021/acs.jpcc.6b12950.*